Version of Record: https://www.sciencedirect.com/science/article/pii/S0021999119308411
Manuscript_40a74026e1e77f7e78d109421624dd1a

Adaptive activation functions accelerate convergence in deep and physics-informed neural networks

Ameya D. Jagtap[1], Kenji Kawaguchi[2] and George Em Karniadakis[1,3,*]

[1]*Division of Applied Mathematics, Brown University, 182 George Street, Providence, RI 02912, USA.*
[2]*Massachusetts Institute of Technology, 77 Massachusetts Ave, Cambridge, MA 02139, USA.*
[3]*Pacific Northwest National Laboratory, Richland, WA 99354, USA.*

Abstract

We employ adaptive activation functions for regression in deep and physics-informed neural networks (PINNs) to approximate smooth and discontinuous functions as well as solutions of linear and nonlinear partial differential equations. In particular, we solve the nonlinear Klein-Gordon equation, which has smooth solutions, the nonlinear Burgers equation, which can admit high gradient solutions, and the Helmholtz equation. We introduce a scalable hyper-parameter in the activation function, which can be optimized to achieve best performance of the network as it changes dynamically the topology of the loss function involved in the optimization process. The adaptive activation function has better learning capabilities than the traditional one (fixed activation) as it improves greatly the convergence rate, especially at early training, as well as the solution accuracy. To better understand the learning process, we plot the neural network solution in the frequency domain to examine how the network captures successively different frequency bands present in the solution. We consider both forward problems, where the approximate solutions are obtained, as well as inverse problems, where parameters involved in the governing equation are identified. Our simulation results show that the proposed method is a very simple and effective approach to increase the efficiency, robustness and accuracy of the neural network approximation of nonlinear functions as well as solutions of partial differential equations, especially for forward problems. We theoretically prove that in the proposed method, gradient descent algorithms are not attracted to suboptimal critical points or local minima. Furthermore, the proposed adaptive activation functions are shown to accelerate the minimization process of the loss values in standard deep learning benchmarks using CIFAR-10, CIFAR-100, SVHN, MNIST, KMNIST, Fashion-MNIST, and Semeion datasets with and without data augmentation.

Keywords: Machine learning, bad minima, Inverse problems, Physics-informed neural network, Burgers equation, Klein-Gordon equation, Helmholtz equation, MNIST, CIFAR.

1. Introduction

Neural networks (NNs) have found applications in the context of numerical solution of partial differential equations, integro-differential equations and dynamical systems. Since, a neural network is an universal approximator, thus it is natural to consider the neural network space as an ansatz space of the solution of governing equation. In [26, 28, 19], NNs are successfully used to obtain the approximate solution of partial diferential equations (PDEs). One can also construct the physics-informed learning machine, which makes use of systematically structured prior information about the solution. In the earlier study, Owhadi [22] showed the promising approach of exploiting such prior information to construct physics-informed learning machines for the numerical homogenization problem. Raissi et al [29, 30] employed Gaussian process regression to obtain representation of functionals of linear operators, which not only infer the solution accurately but also provide uncertainty estimates for many physical problems. Further,

[*] Corresponding author Emails: ameya_jagtap@brown.edu (A.D.Jagtap), kawaguch@mit.edu (K. Kawaguchi), george_karniadakis@brown.edu (G.E.Karniadakis)

© 2019 published by Elsevier. This manuscript is made available under the Elsevier user license
https://www.elsevier.com/open-access/userlicense/1.0/

their method was extended to nonlinear problems by Raissi and Karniadakis [26] and Raissi et al [27] in the context of solution inference and system identification. Data-driven turbulence modeling has been developed by Wang *et al.* [36] and Duraisamy & co-workers in a series of papers [42, 23, 13]. Physics-informed neural networks (PINNs) can accurately solve both forward problems, where the approximate solutions of governing equations are obtained, as well as inverse problems, where parameters involved in the governing equation are obtained from the training data [28]. In the PINN algorithm, along with the contribution from the neural network the loss function is enriched by the addition of residual term from the governing equation(s), which act as a penalizing term that constrains the space of admissible solutions. Figure 1 gives a sketch of a PINN algorithm for the Klein-Gordon equation where one can see the neural network along with the supplementary physics-informed part. The loss function is evaluated using the contribution from the neural network part as well as the residual from the governing equation given by physics-informed part. Then, one seeks the optimal values of weights (w) and biases (b) in order to minimize the loss function below certain tolerance ϵ or until a prescribed maximum number of iterations.

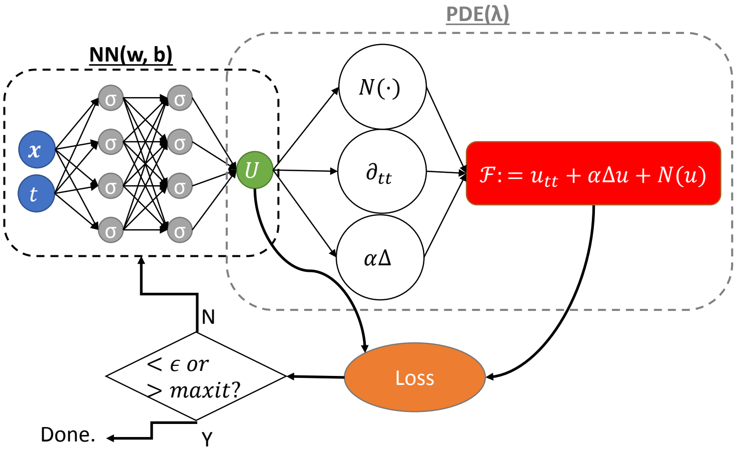

Figure 1: Schematic of PINN for the Klein-Gordon equation. The left NN is the uninformed network while the right one induced by the governing equation is the informed network. The two NNs share hyper-parameters and they both contribute to the loss function.

The activation function plays an important role in such training process due to the dependence of the derivative of loss function on optimization parameters, which, in turn, depends on the derivative of the activation function. In the PINN algorithm various activation functions such as *tanh*, *sin etc* are used to solve various problems, see [28, 31] for more details. There is no obvious choices for the activation function since it solely depends on the problem at hand. To tackle this issue, various methods are proposed in the literature like adaptive sigmoidal activation function for multilayer feedforward NNs proposed by Yu et al [41], while Qian et al [24] focuses on learning activation functions in convolutional NNs via combining basic activation functions in a data-driven way. Dushkoff and Ptucha [14] proposed multiple activation functions per neuron, where individual neurons select between a multitude of activation functions. A tunable activation function is proposed by Li *et al.* [20], where only a single hidden layer is used and the activation function is tuned. In [35], Shen *et al.* used a similar idea of tunable activation function but with multiple outputs.

In this paper the activation function is tuned for any number of hidden layers by introducing an adaptable hyper-parameter with a scaling factor. The behavior of the proposed adaptive activation function with gradient descent algorithms is theoretically analyzed. Along with the deep neural network problem, PINN-based forward and inverse problems involving smooth solutions (like, nonlinear Klein-Gordon equation and Helmholtz equation) as well as steep-gradient solution (Burgers equation) are solved using the proposed method and compared with the fixed activation function. One can clearly see the advantages of using the proposed adaptive activation function such as the increase in the accuracy and fast convergence rate, especially in the early training period. Furthermore, its advantage is empirically demonstrated with standard deep learning benchmark problems.

This paper is organized as follows: After the introduction in section 1, section 2 gives a brief discussion of the proposed methodology, where we also discuss about training data, loss function, optimization methods and the proposed method. We also discuss some theoretical results on the convergence of the proposed method. Section

3 gives the results and detailed discussions on deep neural network approximations of smooth and discontinuous functions as well as PINN based solutions of forward/inverse problems, including the Burgers, Klein-Gordon and Helmholtz equations. Section 4 presents experimental results with various standard deep learning benchmarks using CIFAR-10, CIFAR-100, SVHN, MNIST, KMNIST, Fashion-MNIST, and Semeion datasets with and without data augmentation. Finally, in section 5, we summarize the conclusions of our work.

2. Methodology

We consider a NN of depth D corresponding to a network with an input layer, $D-1$ hidden layers and an output layer. In the k^{th} hidden layer, N_k number of neurons are present. Each hidden layer of the network receives an output $z^{k-1} \in \mathbb{R}^{N_{k-1}}$ from the previous layer where an affine transformation of the form

$$\mathcal{L}_k(z^{k-1}) := w^k z^{k-1} + b^k, \tag{1}$$

is performed. The network weights w^k and bias term b^k associated with the k^{th} layer are chosen from *independent and identically distributed (iid)* samplings. The nonlinear activation function $\sigma(\cdot)$ is applied to each component of the transformed vector before sending it as an input to the next layer. The activation function is an identity function after an output layer. Thus, the final neural network representation is given by the composition

$$u_{\mathbf{\Theta}}(z) = (\mathcal{L}_D \circ \sigma \circ \mathcal{L}_{D-1} \circ \ldots \circ \sigma \circ \mathcal{L}_1)(z),$$

where the operator $\circ$ is the composition operator, $\mathbf{\Theta} = \{w^k, b^k\}_{k=1}^D$ represents the trainable parameters in the network, u is the output and $z^0 = z$ is the input.

2.1. Training data

In the supervised learning, training data is important to train the neural network, which can be obtained from the exact solution (if available) or from high-resolution numerical solution using methods like spectral method, discontinuous Galerkin method *etc*, as per the problem at hand. Here we select the training points either randomly from the uniform/normal distribution or one can also choose these points depending upon the small length and time scales (high gradient regions) present in the solution space. Training data can also be obtained from carefully performed experiments, which may yield both high- and low-fidelity data sets.

2.2. Loss function and optimization algorithm

We aim to find the optimal weights for which the suitably defined loss function is minimized. In PINN the loss function is defined as

$$J(\mathbf{\Theta}) = MSE_{\mathcal{F}} + MSE_u \tag{2}$$

where the mean squared error (MSE) is given by

$$MSE_{\mathcal{F}} = \frac{1}{N_f}\sum_{i=1}^{N_f} |\mathcal{F}(x_f^i, y_f^i, t_f^i)|^2, \qquad MSE_u = \frac{1}{N_u}\sum_{i=1}^{N_u} |u^i - u(x_u^i, y_u^i, t_u^i)|^2.$$

Here $\{x_f^i, y_f^i, t_f^i\}_{i=1}^{N_f}$ denotes the residual training points in the space-time domain and $\{x_u^i, y_u^i, t_u^i\}_{i=1}^{N_u}$ denotes the boundary/initial training data. The aim of including the first term is that the neural network solution must satisfy the governing equation at randomly chosen points in the domain, which constitutes the physics-informed part of neural network whereas the second term includes the known boundary/initial conditions, which must be satisfied by the neural network solution. The resulting optimization problem leads to finding the minimum of a loss function by optimizing the parameters, *i.e.*, we seek to find

$$w^* = \underset{w \in \mathbf{\Theta}}{\arg\min}\ (J(w)); \qquad b^* = \underset{b \in \mathbf{\Theta}}{\arg\min}\ (J(b)).$$

One can approximate the solutions to this minimization problem iteratively by one of the forms of gradient descent algorithm. The stochastic gradient descent (SGD) algorithm is widely used in machine learning community, see [33] for a survey. In SGD the weights are updated as

$$w^{m+1} = w^m - \eta_l \nabla_{w^m} J^m(w)$$

where $\eta_l > 0$ is the learning rate and J^m is the loss function at m^{th} iteration. SGD methods can be initialized with some starting value w^0. In this work, the ADAM optimizer [17], which is a variant of the SGD method is used in all problems.

2.3. Adaptive activation functions

In the literature, various activation functions are available such as sigmoid or logistic, tanh. ReLU, Leaky-ReLU *etc* [15]. The role of activation function is to decide whether particular neuron should fire or not. When the activation function is absent the weights and bias would simply do a linear transformation, which is a case of a linear regression model. Such linear model is simple to solve but is limited in its capacity to solve complex problems. The nonlinear activation function performs the nonlinear transformation to the input data making it capable to learn and perform more complex tasks. In the back-propagation algorithm, the evaluation of gradient of the loss function involves the gradient of the activation function. Activation functions make the back-propagation possible since the gradients are supplied to update the weights and biases; hence, without the differentiable nonlinear activation function, this would not be possible. Thus, one must choose an activation function which is less prone to the *vanishing* and the *exploding* gradient problem [6]. In this work, we have tried different activation functions, and their performance is compared in the results and discussion section.

The size of a network is correlated to its capacity to reproduce complicated functions. A deep network is required to solve complex problems, which on the other hand is difficult to train. In most cases, a suitable architecture is selected based on the researcher's experience, which is a trial and error based method. One can think of tuning the network to get the best performance out of it. To achieve this, we introduce the hyper-parameter a in the activation function as

$$\sigma(a \, \mathcal{L}_k(z^{k-1})),$$

which needs to be optimized. The resulting optimization problem leads to finding the minimum of a loss function by optimizing a along with the weights and biases, *i.e.*, we seek to find

$$a^* = \underset{a \in \mathbb{R}^+ \setminus \{0\}}{\arg\min} \; (J(a)).$$

The parameter a is updated as

$$a^{m+1} = a^m - \eta_l \nabla_{a^m} J^m(a).$$

Mathematically, such hyper-parameter can change the slope of the activation function, which is one of the important aspects of the neural network training. Figure 2 shows the sigmoid, tanh, ReLU and Leaky-ReLU activation functions with different values of hyper-parameter a, where we can see the changes in slope of the activation function with a. The corresponding expressions of these activation function are given by

$$\begin{aligned} \text{Sigmoid} : &\; \frac{1}{1+e^{-ax}}, \\ \text{Hyperbolic tangent} : &\; \frac{e^{ax}-e^{-ax}}{e^{ax}+e^{-ax}}, \\ \text{ReLU} : &\; \max(0, ax), \\ \text{Leaky ReLU} : &\; \max(0, ax) - \nu \, max(0, -ax). \end{aligned}$$

The learning rate has a great impact while searching for global minima. Large learning rate can over-shoot the global minima whereas small learning rate can increase the computational cost although it slowly moves towards global minima. The common practice is to use small learning rate for such optimization problem, which gives slow

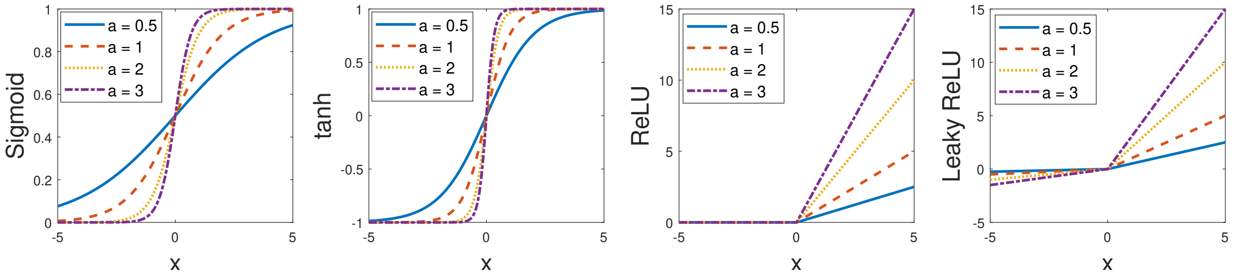

Figure 2: (Left to right) Sigmoid or logistic, tanh, ReLU and Leaky-ReLU activation functions for various values of a.

variation or say slow convergence towards the optimized value. Intuitively, one can think of some scale factor $n \geq 1$ multiplied by a, which accelerates convergence towards global minima. Thus, the final form of the activation function is given by

$$\sigma(na\,\mathcal{L}_k(z^{k-1})).$$

It is important to note that the introduction of the scalable hyper-parameter does not change the structure of loss function defined previously. Then, the final adaptive activation function based neural network representation is given by

$$u_{\tilde{\mathbf{\Theta}}}(z) = (\mathcal{L}_D \circ \sigma \circ na\mathcal{L}_{D-1} \circ \sigma \circ na\mathcal{L}_{D-2} \circ \ldots \circ \sigma \circ na\mathcal{L}_1)(z).$$

In this case, the trainable parameters are $\tilde{\mathbf{\Theta}} = \{w^k, b^k, a\}_{k=1}^{D}$. Compared to the original neural network, the adaptive activation function based PINN has one additional scalable hyper-parameter a to train. The adaptive activation function based PINN algorithm is summarized as follows.

Algorithm 1: Adaptive activation function based PINN algorithm

```
**Step 1** : Specification of training set
Training data : $u_{NN}$ network $\{x_u^i, y_u^i, t_u^i\}_{i=1}^{N_u}$.
Residual training points : $\mathcal{F}$ network $\{x_f^i, y_f^i, t_f^i\}_{i=1}^{N_f}$.
**Step 2** : Construct neural network $u_{NN}(\tilde{\mathbf{\Theta}})$ with random initialization of parameters $\tilde{\mathbf{\Theta}}$.
**Step 3** : Construct the residual neural network $\mathcal{F}$ by substituting surrogate $u_{NN}$ into the governing equations
  using automatic differentiation [5] and other arithmetic operations.
**Step 4**: Specification of loss function:
    $J(\tilde{\mathbf{\Theta}}) = \frac{1}{N_f}\sum_{i=1}^{N_f} |\mathcal{F}(x_f^i, y_f^i, t_f^i)|^2 + \frac{1}{N_u}\sum_{i=1}^{N_u} |u^i - u(x_u^i, y_u^i, t_u^i)|^2.$
**Step 5**: Find the best parameters using suitable optimization method for minimizing the loss function
    $\tilde{\mathbf{\Theta}}^* = \arg\min\,(\tilde{\mathbf{\Theta}}).$
```

We now provide a theoretical result regarding the proposed method. The following theorem states that a gradient descent algorithm minimizing our objective function $J(\tilde{\mathbf{\Theta}})$ with a L2 regularization does not converge to a suboptimal critical point or local minimum with an appropriate initialization and learning rates. Let $J_\zeta(\tilde{\mathbf{\Theta}}) = J(\tilde{\mathbf{\Theta}}) + \zeta\|\mathbf{\Theta}\|_2^2$ (i.e., the objective function with the L2 regularization) where $\zeta > 0$ is a fixed hyper-parameter (the value of which can be arbitrary) and we treat $\mathbf{\Theta}$ as a vector in $\mathbb{R}^\tau$ (τ is the total number of parameters) and $\tilde{\mathbf{\Theta}}$ as a vector in $\mathbb{R}^{\tau+1}$.

Theorem 2.1. *Let $(\tilde{\mathbf{\Theta}}_m)_{m\in\mathbb{N}}$ be a sequence generated by a gradient descent algorithm as $\tilde{\mathbf{\Theta}}_{m+1} = \tilde{\mathbf{\Theta}}_m - \eta_m \nabla J_\zeta(\tilde{\mathbf{\Theta}})$. Assume that $J_\zeta(\tilde{\mathbf{\Theta}}_0) < J_\zeta(0)$, J_ζ is differentiable, and that for each $i \in \{1, \ldots, N_f\}$, there exist differentiable function φ^i*

and input ρ^i such that $|\mathcal{F}(x_f^i, y_f^i, t_f^i)|^2 = \varphi^i(u_{\Theta}(\rho^i))$. Assume that at least one of the following three conditions holds.

(i) *(constant learning rate) ∇J_ζ is Lipschitz continuous with Lipschitz constant C (i.e., $\|\nabla J_\zeta(\tilde{\mathbf{\Theta}}) - \nabla J_\zeta(\tilde{\mathbf{\Theta}}')\|_2 \leq C\|\tilde{\mathbf{\Theta}} - \tilde{\mathbf{\Theta}}'\|_2$ for all $\tilde{\mathbf{\Theta}}, \tilde{\mathbf{\Theta}}'$ in its domain), and $\epsilon \leq \eta_m \leq (2-\epsilon)/C$, where ϵ is a fixed positive number.*

(ii) *(diminishing learning rate) ∇J_ζ is Lipschitz continuous, $\eta_m \to 0$ and $\sum_{m=0}^{\infty} \eta_m = \infty$.*

(iii) *(adaptive learning rate) the learning rate η_m is chosen by the minimization rule, the limited minimization rule, the Armjio rule, or the Goldstein rule [8].*

Then, no limit point of $(\tilde{\mathbf{\Theta}}_m)_{m\in\mathbb{N}}$ is a suboptimal critical point or local minimum.

The proof of Theorem 2.1 is deferred to the appendix A.

3. Results and discussion

In this section, first we shall approximate nonlinear smooth and discontinuous functions using neural networks with fixed and adaptive activations. Subsequently, we will solve Burgers, Klein-Gordon and Helmholtz equations, which can admit both continuous as well as high gradient solutions using PINNs with fixed and adaptive activations. Both forward problems, where the solution is inferred, as well as inverse problems, where the parameters involved in the governing equation are obtained using the proposed adaptive activation function based PINN. To show the effectiveness of the proposed method, various comparisons are made. In this study, the optimal value of learning rate is found by experiments to be 0.0008.

3.1. Neural network approximation of nonlinear smooth and discontinuous functions

In this test case we are using a standard NN (without physics-informed part) to approximate smooth and discontinuous functions. In this case the loss function consists of just a neural network part given by

$$J(\tilde{\mathbf{\Theta}}) = \frac{1}{N_u}\sum_{i=1}^{N_u} |u^i - u(x_u^i, y_u^i, t_u^i)|^2.$$

The activation function is *tanh* and the number of hidden layers is four with 50 neurons in each layer.

Here, we shall consider two smooth functions and one discontinuous function. First, the smooth function is given by

$$u(x) = (x^3 - x)\,\frac{\sin(7x)}{7} + \sin(12x), \quad x \in [-3,\ 3]. \tag{3}$$

In this function both high and low frequency components are present. The number of training points N_u used is 300. Next, we consider the Burgers equation given by

$$u_t + uu_x = \tilde{\epsilon}u_{xx}, \quad x \in [-1,\ 1], \ t > 0 \tag{4}$$

with initial condition $u(x, 0) = -\sin(\pi x)$, boundary conditions $u(-1, t) = u(1, t) = 0$ and $\tilde{\epsilon} = 0.01/\pi$. The analytical solution can be obtained using the Hopf-Cole transformation, see Basdevant et al., [3] for more details. We consider the smooth solution of Burgers equation at time $t = 0.25$ to be approximated by a deep neural network. The number of training points used is 256.

Finally, the following discontinuous function with discontinuity at $x = 0$ location is approximated by a deep neural network.

$$u(x) = \begin{cases} 0.2\ \sin(6x) & \text{If } x \leq 0 \\ 1 + 0.1\ x\cos(12x) & \text{Otherwise.} \end{cases} \tag{5}$$

Here, the domain is $[-4,\ 3.75]$. In this case, the number of training points used is 300.

Knowledge of training process of neural network is important in order to optimize this process. In the earlier study, Arpit, *et al.* [1] suggested that the neural network learns simple pattern first before memorizing. Similar results have

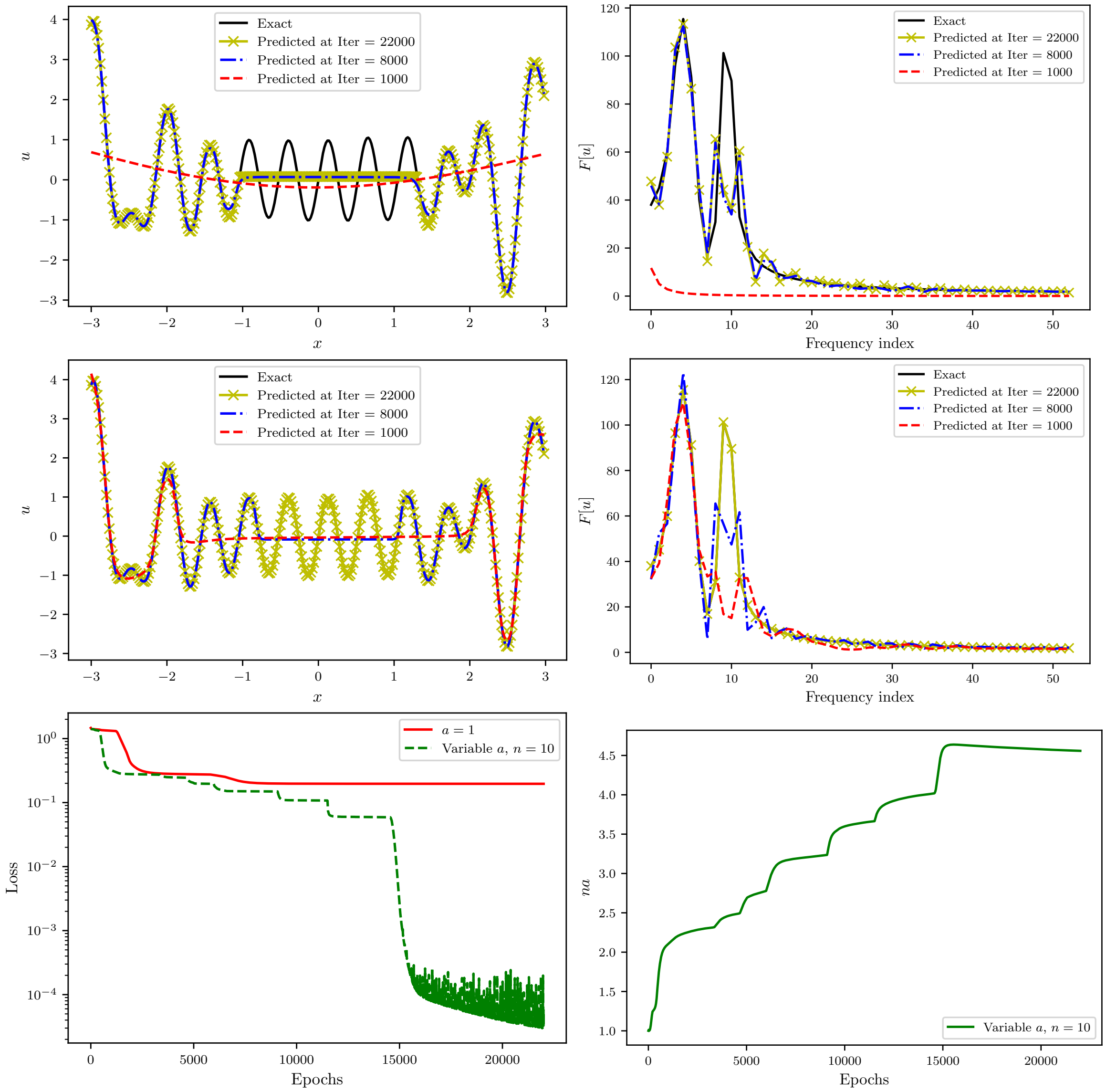

Figure 3: Smooth function: Neural network solution of fixed (top row) and adaptive activation (middle row) functions. First column (top and middle row) shows the solution, which is also plotted in frequency domain (zoomed-view) as shown by the corresponding second column. Bottom row shows the loss function comparison for fixed and adaptive activation (left) and variation in a with $n = 10$ (right).

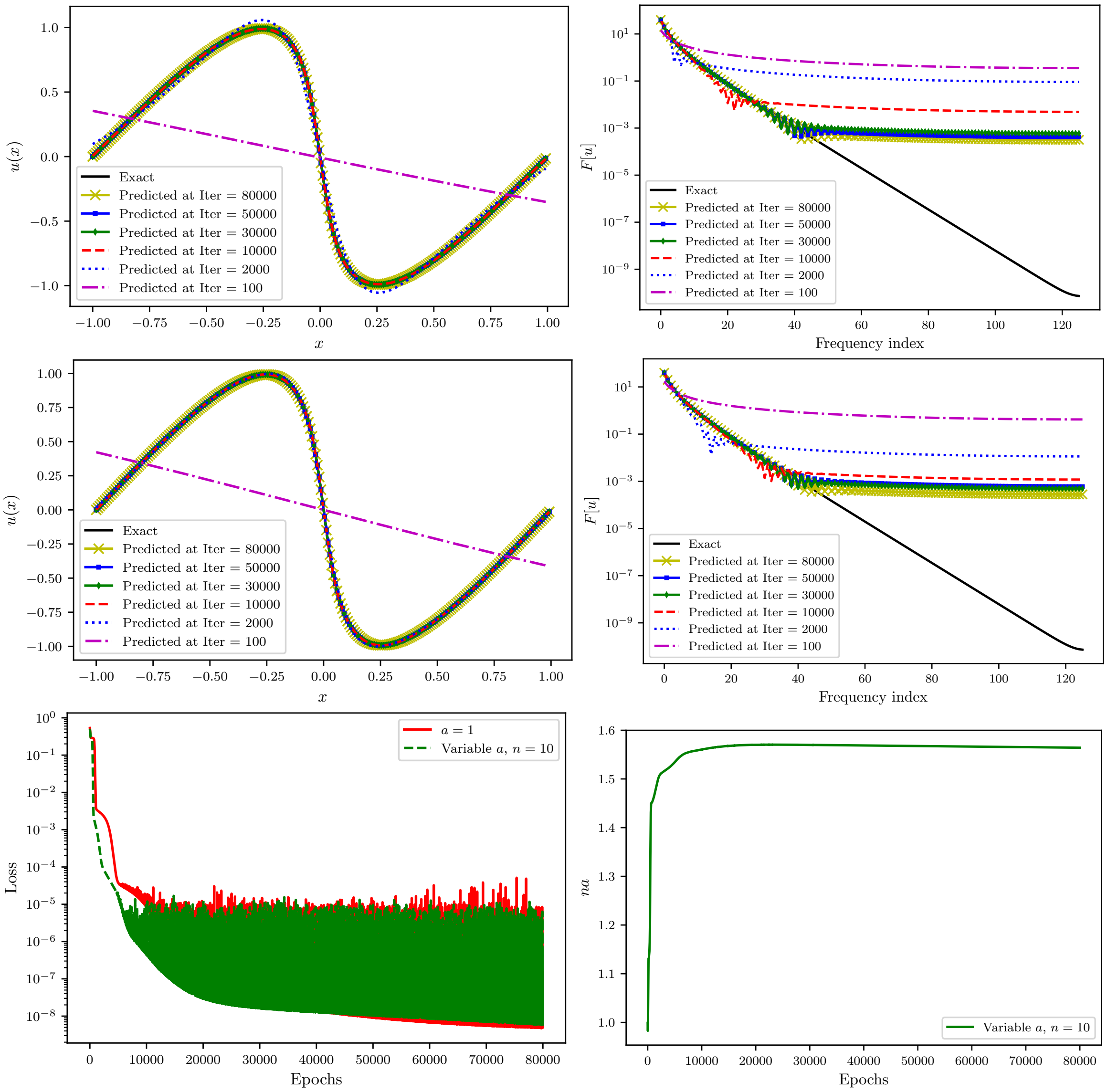

Figure 4: Smooth Burgers solution: Neural network solution of fixed (top row) and adaptive activation (middle row) functions. First column (top and middle row) shows the solution which is also plotted in frequency domain as shown by the corresponding second column. Bottom row shows the loss function comparison for fixed and adaptive activation (left) and variation in a with $n = 10$ (right).

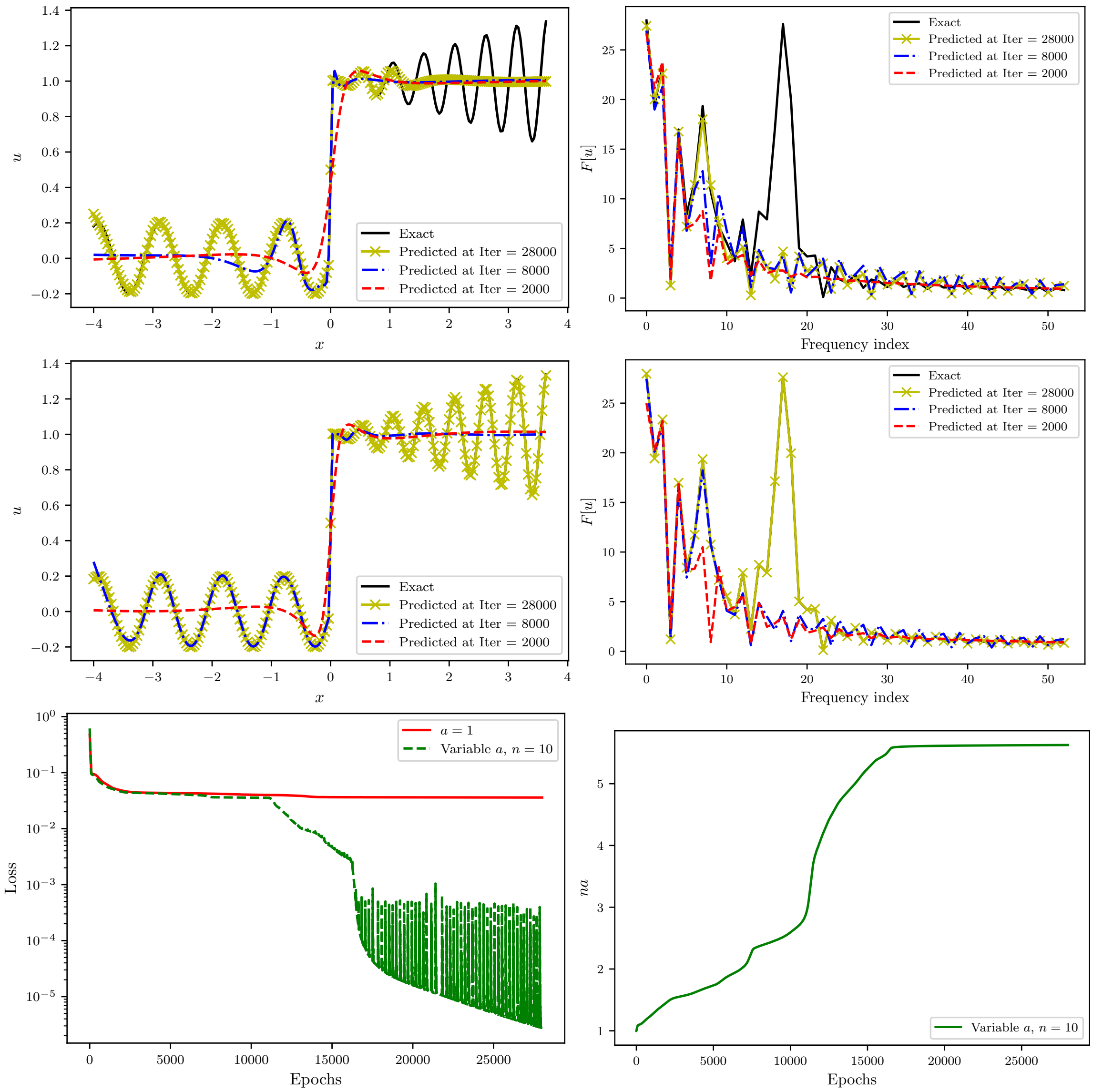

Figure 5: Discontinuous function: Neural network solution of fixed (top row) and adaptive activation (middle row) functions. First column (top and middle row) shows the solution which is also plotted in frequency domain (zoomed-view) as shown by the corresponding second column. Bottom row shows the loss function comparison for fixed and adaptive activation (left) and variation in a with $n = 10$ (right).

been found by Rahaman, *et al.* [25], who suggested that the neural network learns low frequencies first. They showed that the amplitude of each frequency component of the network output is controlled by the spectral norm of the small-size network, which increases gradually during the training process. Thus, longer training time allows the network to learn complex functions by allowing it to capture the high frequencies components in the solution. Another such tool is the *frequency principle* or *F-principle* proposed by Xu, *et al.*, see [39] and the references therein. In this case, the evolution of solution is observed in frequency domain by taking the Fourier transform $F[u]$ of a solution, where one can see that the neural network captures the low frequency first during the training process and then captures high frequency components. In this work, we shall use the F-principle to observe the performance of adaptive activation function.

Figure 3 shows the smooth solution given by fixed (top row) and adaptive activation (middle row) functions. The first column (top and middle rows) shows the solutions whereas the second column (top and middle rows) shows the solution in frequency domain. The adaptive activation function captures all frequencies in 22000 iterations as opposed to fixed activation. This behavior is also reflected in their solution plots. The bottom left figure shows the loss function comparison for fixed and adaptive activation with scaling factor 10. The loss is decreasing faster in case of adaptive activation and the optimal value of a is around 4.5 as shown in the bottom right figure. The neural network tries to capture the low frequency first and then high frequency components, which can be seen from the solution as well as from the corresponding frequency plots.

Figure 4 shows the smooth Burgers solution given by fixed (top row) and adaptive activation (middle row) functions. The first column (top and middle rows) shows the solutions whereas the second column (top and middle rows) shows the solution in frequency domain. We observe that even after 80000 iterations we are unable to capture all frequencies in the solution. Nonetheless, the adaptive activation function captures the frequencies faster than the fixed activation. The bottom left figure shows the loss function comparison for fixed and adaptive activation with scaling factor 10. The loss is decreasing faster in the case of adaptive activation and the optimal value of a is around 1.56 as shown in the bottom right figure.

Finally, figure 5 shows the discontinuous solution given by fixed (top row) and adaptive activation (middle row) functions. The first column (top and middle rows) shows the solutions whereas the second column (top and middle rows) shows the solution in frequency domain. The adaptive activation function captures all frequencies in 28000 iterations whereas the fixed activation function fails to capture these frequencies, which can be also be seen from their solution plots. The bottom left figure shows the loss function comparison for fixed and adaptive activation with $n = 10$. The loss is decreasing faster in the case of adaptive activation. Finally, the bottom right figure gives the variation of na, which gives the optimal value around 5.86. In this case, the neural network first captures the discontinuity and then low frequency components present in $x < 0$ region and finally captures the high frequencies present in $x > 0$ region.

3.2. Burgers equation

The Burgers equation is one of the fundamental partial differential equation arising in various fields such as nonlinear acoustics, gas dynamics, fluid mechanics *etc*, see Whitham [38] for more details. The Burgers equation was first introduced by H. Bateman [4] and later studied by J.M. Burgers [9] in the context of theory of turbulence. The inviscid Burgers equation is a nonlinear first-order hyperbolic partial differential equation, which can develop discontinuities even when the initial condition is sufficiently smooth. Here, in the case of vanishing viscosity, we shall consider Burgers equation given by equation (4) along with its initial and boundary conditions. The nonlinearity in the convection term develops very steep solution due to small $\tilde{\epsilon}$ value. The number of training data points on the boundary is 400, the number of residual training points is 10000 and

$$\mathcal{F} := (u_{NN})_t + u_{NN}(u_{NN})_x - \tilde{\epsilon}(u_{NN})_{xx},$$

where u_{NN} represents solution given by NN. The neural network architecture used for the computation consists of six hidden layers with 20 neurons in each layer.

Figure 6 shows the contour plot of the solution of the Burgers equation and figure 7 shows the comparison of exact and PINN solutions of Burgers equation with $\tilde{\epsilon} = 0.01/\pi$. In the top figure, the fixed activation function without any tuning parameters is used where the value of a is unity. The middle and bottom figures present the results of adaptive activation function, where a is a variable and scaling factors $n = 1$ and 5 are used in the respective figures. By

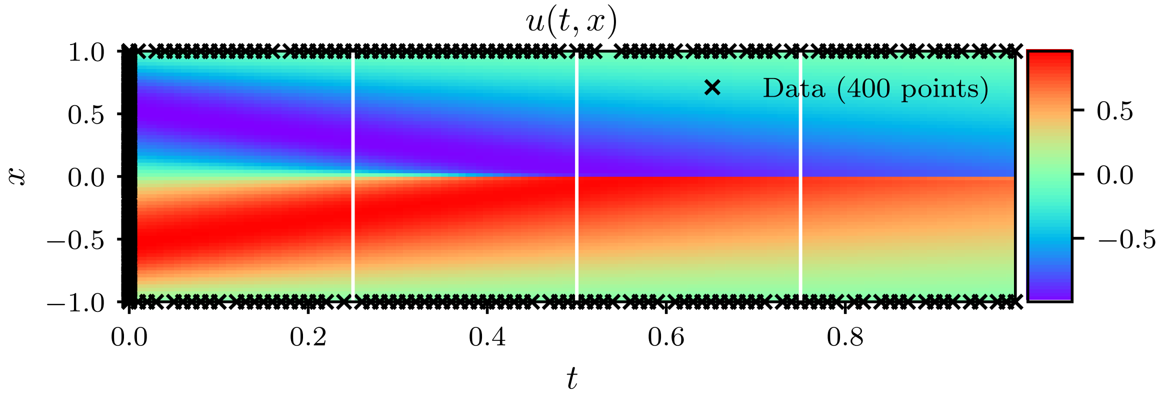

Figure 6: Solution of Burgers equation (after 2000 iterations) on $x-t$ domain with variable $a, n = 5$. The three vertical white lines indicate the locations where the exact solution is compared with the solution given by PINN in figure 7

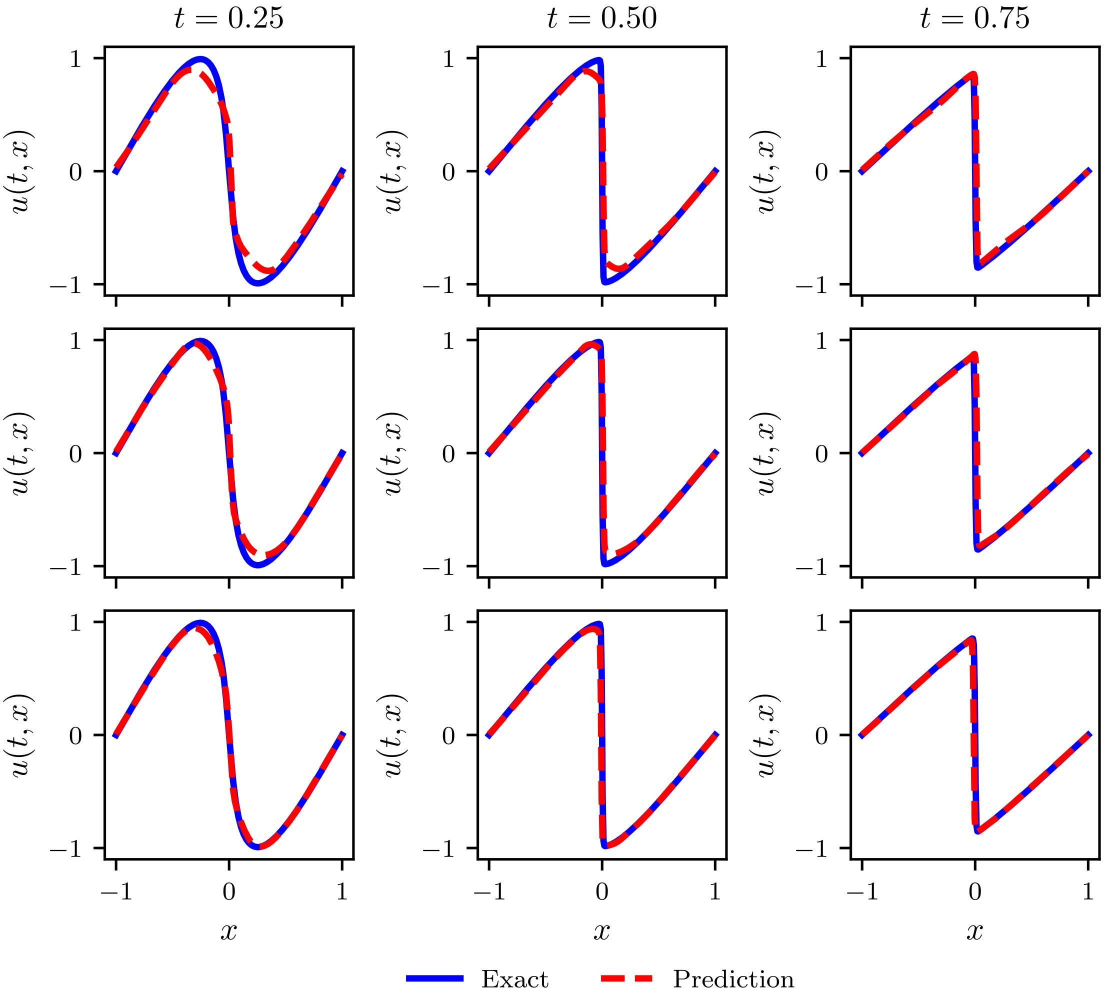

Figure 7: Burgers equation: Comparison of the exact solution with the solution given by PINN using $a = 1$ (top), variable $a, n = 1$ (middle) and variable $a, n = 5$ (bottom) obtained after 2000 iterations.

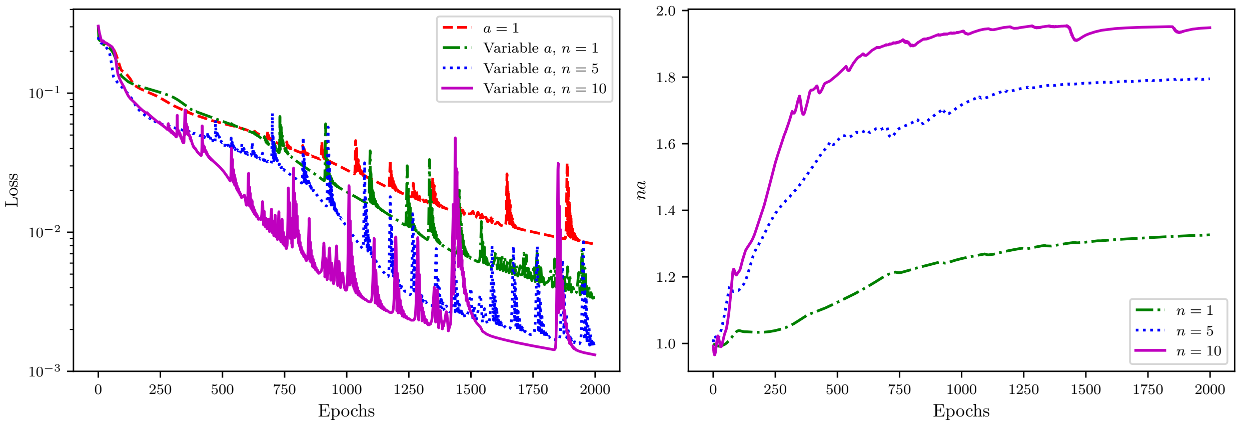

Figure 8: Burgers equation: Loss vs. epochs for fixed and variable a with different values of n (left) and corresponding variation in na with epochs (right).

introducing the adjustable parameter, the accuracy of the solution improves. Figure 8 (left) shows the variation of the loss function with epochs, where we can see the effect of hyper-parameter introduced in the activation function. For variable a, the loss function converges faster with increasing scaling factor as compared to fixed activation function.

Figure 8 (right) shows the optimization process for variable a. For unity scaling factor the optimization process of a is slow due to small learning rate. One can increase the speed of tuning process further by increasing the scaling factor as shown in figure. Table 1 gives the relative L_2 error for fixed as well as adaptive activation function, where it can be observed that the error decreases with increasing scaling factor.

	$a = 1$	Variable a, $(n = 1)$	Variable a, $(n = 5)$	Variable a, $(n = 10)$
Relative L_2 error	1.913973e-01	1.170261e-01	9.928848e-02	9.517134e-02

Table 1: Burgers equation: Relative L_2 error after 2000 iterations with different values of a with clean data.

To show the comparison of fixed and adaptive activation functions we plotted the neural network solution of Burgers equation at $t = 0.25, 0.5$ and 0.75 (column-wise) in frequency domain and compared their results. Figure 9 shows the results for ReLU activation function. The first row shows the fixed activation function whereas the second row gives result for the adaptive activation. In both cases, activation is unable to capture the frequencies present in the solution. Thus, ReLU is not a good activation function for this problem. Next, we used *'tanh'* activation and figure 10 shows the corresponding results. In the case of adaptive activation function, the process of capturing the correct frequency is faster than the fixed activation function for $t = 0.5$ and 0.75. From the middle figures (top and bottom), the adaptive activation function captures almost all frequencies compared to fixed activation in a short duration. Similar behavior can be observed from the right figures (top and bottom) where dominant frequencies are captured in just 1000 iterations using the adaptive activation shown by blue curve (dash-dot line). Figure 11 shows the results for *'sin'* activation function where a similar trend can be seen in the solution for both activation functions at $t = 0.5$ and 0.75. In the case of smooth solution at $t = 0.25$ all activation functions fail to capture the frequencies present in the solution. This is clear from our previous example of approximating the smooth Burgers solution at $t = 0.25$ using NN requiring a large number of iterations to capture all frequencies present in the solution.

The introduction of a scalable hyper-parameter in the activation function dynamically changes the topology of the loss function thereby achieving faster convergence towards global minima. Figure 12 (top row) shows the initial and final optimized *'tanh'* (left) and *'sin'* (right) activation functions. The corresponding *activation planes ($na - x$ plane)* and *activation surfaces* are given by the middle and bottom rows, respectively. In both cases we observe that the gradient of the activation function increases from its initial stage in the direction of large values of na, which contributes towards the fast learning process of the neural network.

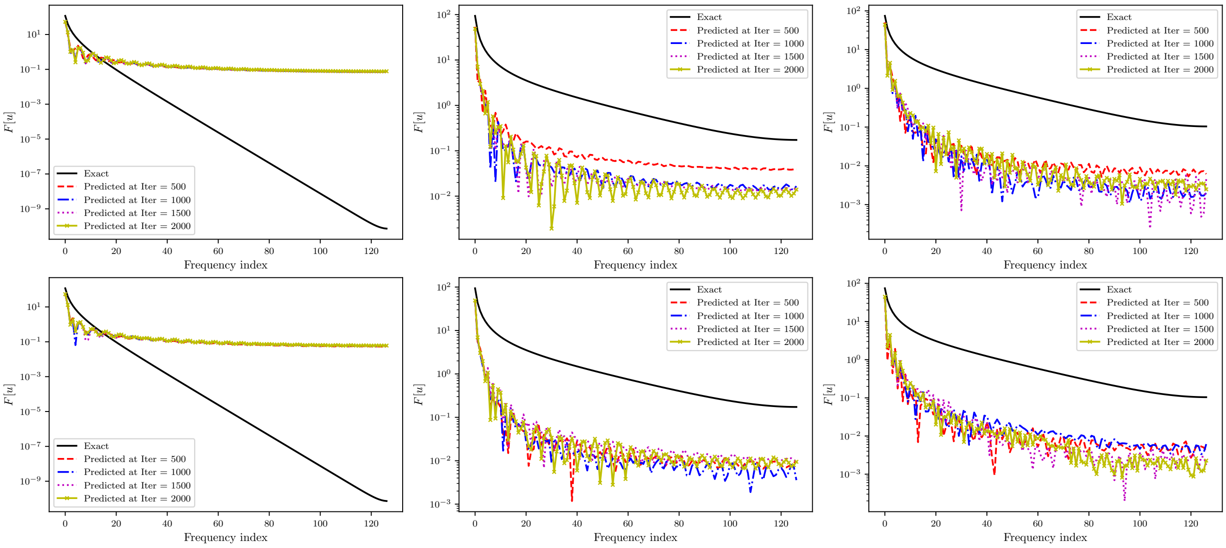

Figure 9: ReLU activation: Comparison of solution of Burgers equation in frequency domain with fixed (1st row) and variable $a, n = 5$ (2nd row) *'ReLU'* activation function. Columns (left to right) represent the solution in frequency domain at $t = 0.25, 0.5$ and 0.75, respectively.

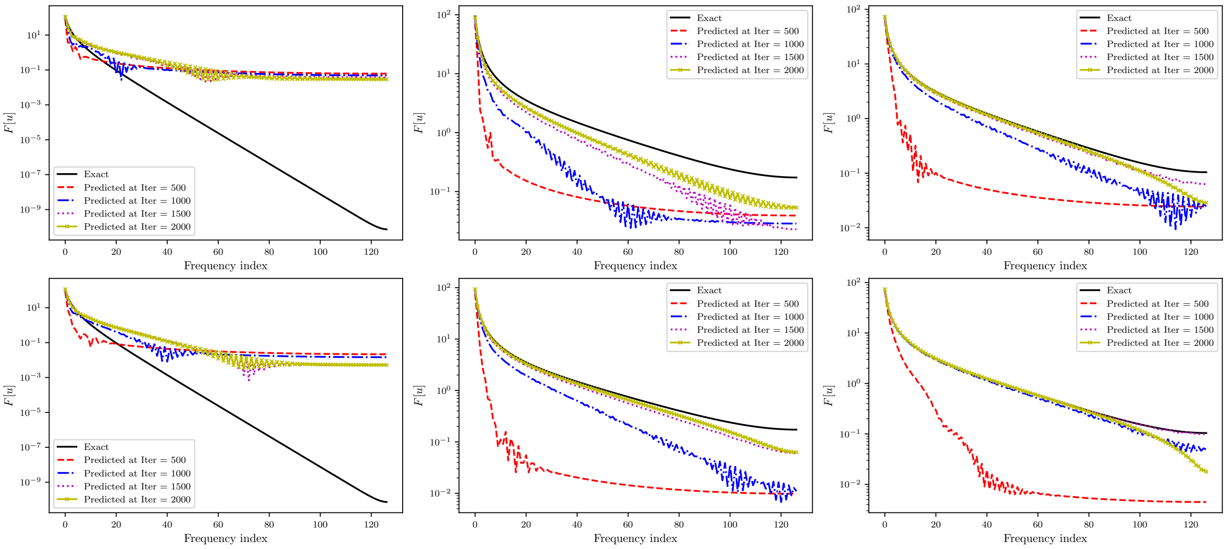

Figure 10: *'Tanh'* activation: Comparison of solution of Burgers equation in frequency domain with fixed (1st row) and variable $a, n = 5$ (2nd row) *'tanh'* activation function. Columns (left to right) represent the solution in frequency domain at $t = 0.25, 0.5$ and 0.75, respectively.

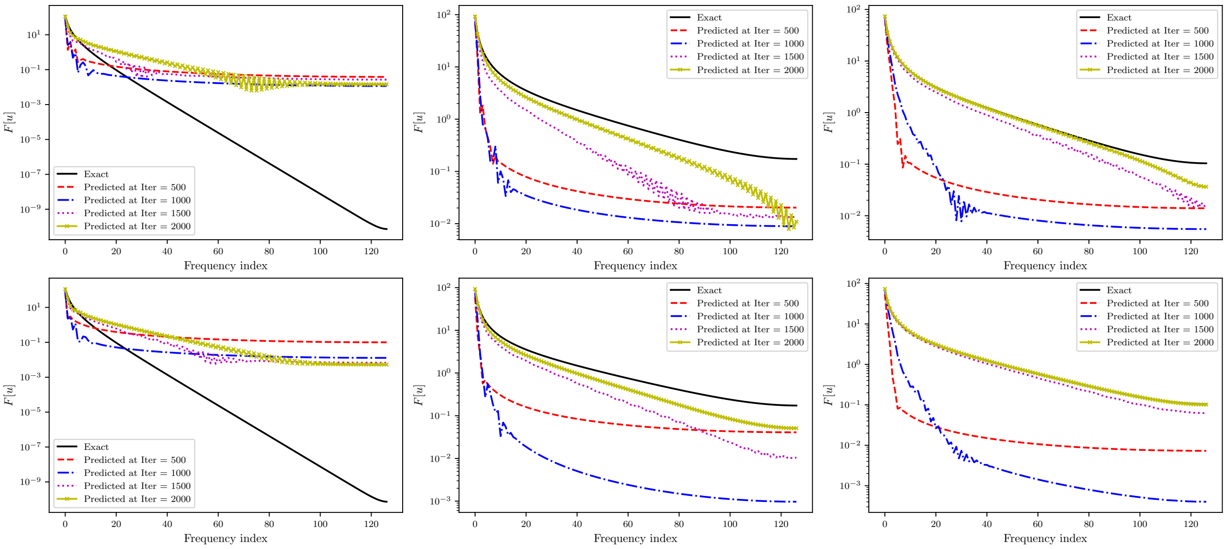

Figure 11: *'Sin'* activation: Comparison of solution of Burgers equation in frequency domain with fixed (1st row) and variable $a, n = 5$ (2nd row) *'sin'* activation function. Columns (left to right) represent the solution in frequency domain at $t = 0.25, 0.5$ and 0.75, respectively.

3.2.1. Initialization of scaled hyper-parameter and effect of large scaling factor

Initialization of the scaled hyper-parameter can be done in various ways as long as such value does not cause divergence of the loss. In this work the scaled hyper-parameter is initialized as $na = 1, \ \forall n \geq 1$. Although, increase in scaling factor speeds up the convergence rate, at the same time the parameter a becomes more sensitive. This can be seen from the oscillations in the loss function as well as in the values of a, figure 8 (right). The reason behind this is that the SGD optimization algorithm becomes very sensitive, hence we should not use a large scaling factor which may eventually cause the solution to diverge. To overcome this difficulty we can think of adding a regularization term in the loss function. Although it partially suppresses the oscillations in the loss function, the other fatal effect of this addition is deterioration of convergence rate, which also reduces the accuracy of the solution. We can also add this regularization term after some iterations (instead of initially), which may nullify the effect of slower convergence rate but still we may not get rid of oscillations fully. Moreover, finding the correct value of regularization weight is still based on trial and error analysis.

3.3. Klein-Gordon equation

The nonlinear Klein-Gordon equation is a second-order hyperbolic partial differential equation arising in many scientific fields like soliton dynamics and condensed matter physics [10], solid state physics, quantum field theory and nonlinear optics [37], nonlinear wave equations [12] *etc*. The inhomogeneous Klein-Gordon equation is given by

$$u_{tt} + \alpha\Delta u + N(u) = h(x,t), \quad x \in [-1, \ 1], \ \ t > 0, \tag{6}$$

where initial conditions and boundary condition are extracted from the exact solution given by $u(x,t) = x\cos(t)$. Δ is a Laplacian operator and $N(u) = \beta u + \gamma u^k$ is the nonlinear term with quadratic nonlinearity ($k = 2$) and cubic non-linearity ($k = 3$); α, β, γ are constants.

Now, let us consider the one-dimensional test case where the computational domain is $[-1, \ 1]$, the initial conditions are $f(x) = x, \ \ g(x) = 0$ with $\alpha = -1, \beta = 0, \gamma = 1, \ k = 2$ and $h(x,t) = -x\cos(t) + x^2\cos^2(t)$. The number of training data points on the boundary is 500, the number of residual training points is 10000 and

$$\mathcal{F} := u_{tt} - \Delta u_{NN} - N(u_{NN})$$

The neural network architecture used for the computation consists of two hidden layers with 40 neurons in each layer. Figure 13 shows the contour plot of the solution of Klein-Gordon equation and figure 14 shows the comparison of

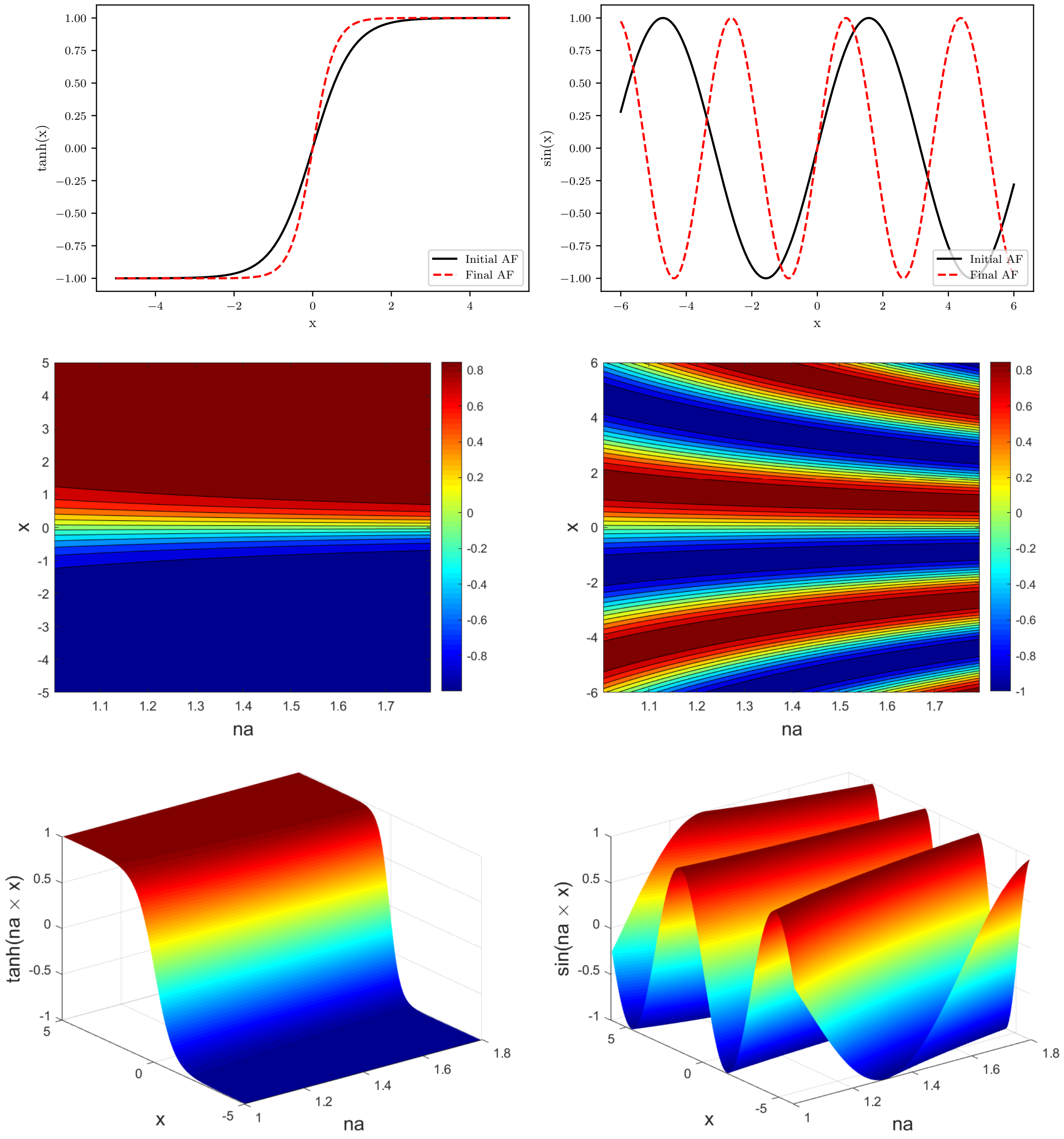

Figure 12: Burgers equation: (Top row) Initial and final *tanh* (left) and *sin* (right) activation functions, (middle row) *tanh* (left) and *sin* (right) activation plane which shows the variation of activation function with *a* and (bottom row) shows corresponding activation surfaces.

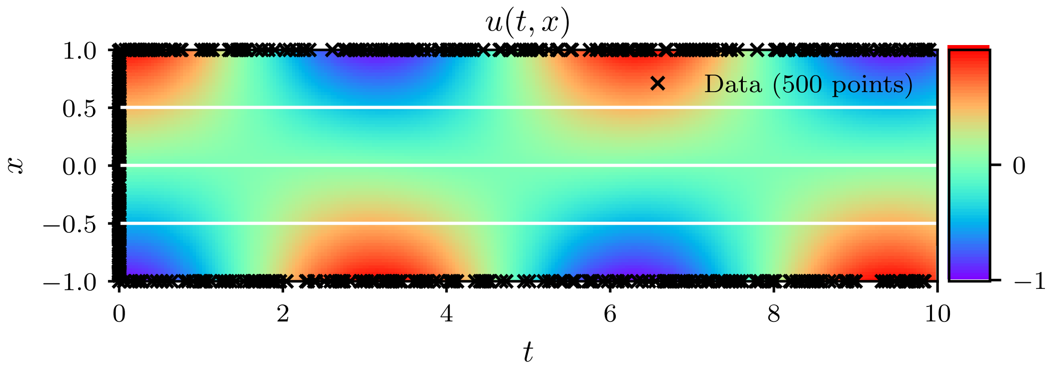

Figure 13: Solution of the Klein-Gordon equation (after 1400 iterations) given by PINN using the adaptive activation function with variable $a, n = 5$. The three white horizontal lines indicate the locations where the exact solution is compared with the solution given by PINN in figure 14.

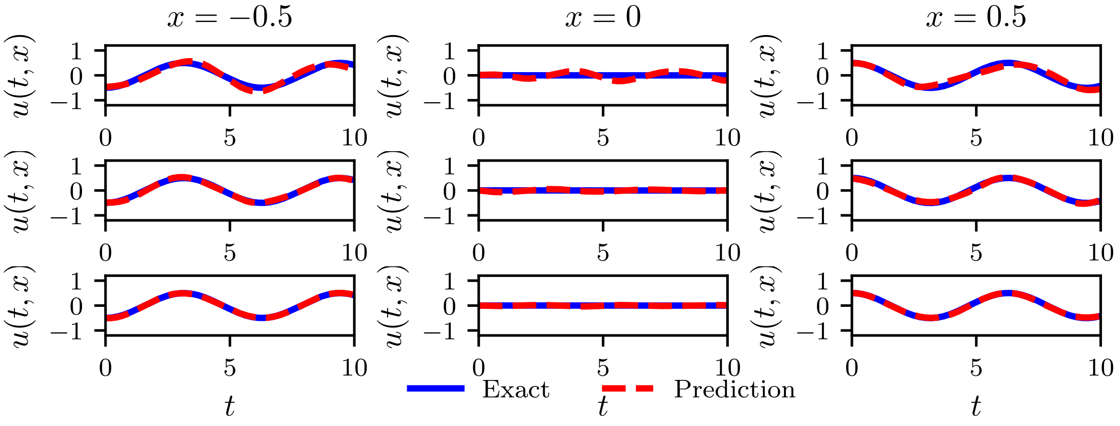

Figure 14: Klein-Gordon equation: Comparison of the exact solution with the solution given by PINN using $a = 1$ (top), variable $a, n = 1$ (middle) and variable $a, n = 5$ (bottom) obtained after 1400 iterations.

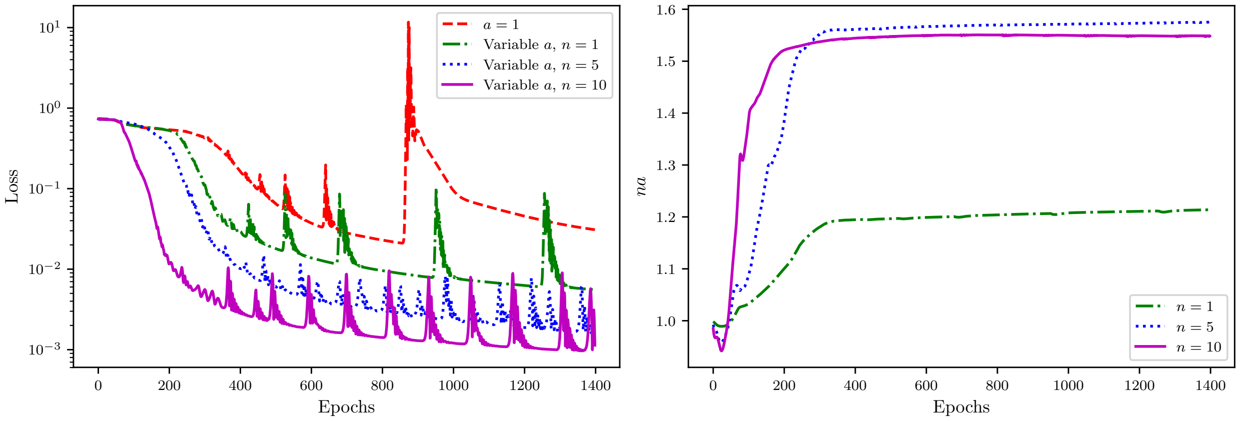

Figure 15: Klein-Gordon equation: Loss vs. epochs for the fixed and variable a with different values of n (left) and corresponding variation in na with epochs (right).

exact and PINN solutions with fixed activation function (top) and adaptive activation function with variable a and $n = 1$ (middle) and $n = 5$ (bottom). There is no difference in solution for $n = 5$ and 10, hence plotted the solution for $n = 5$ only. In these figures we can see that the solution is improving with increasing n. Figure 15 (left) shows the loss function with epochs. Again, convergence is faster for the adaptive activation function with increasing n. Also, the value of a converges to optimized value, which is nearly 1.548 with increasing scaling factor as shown in figure 15 (right).

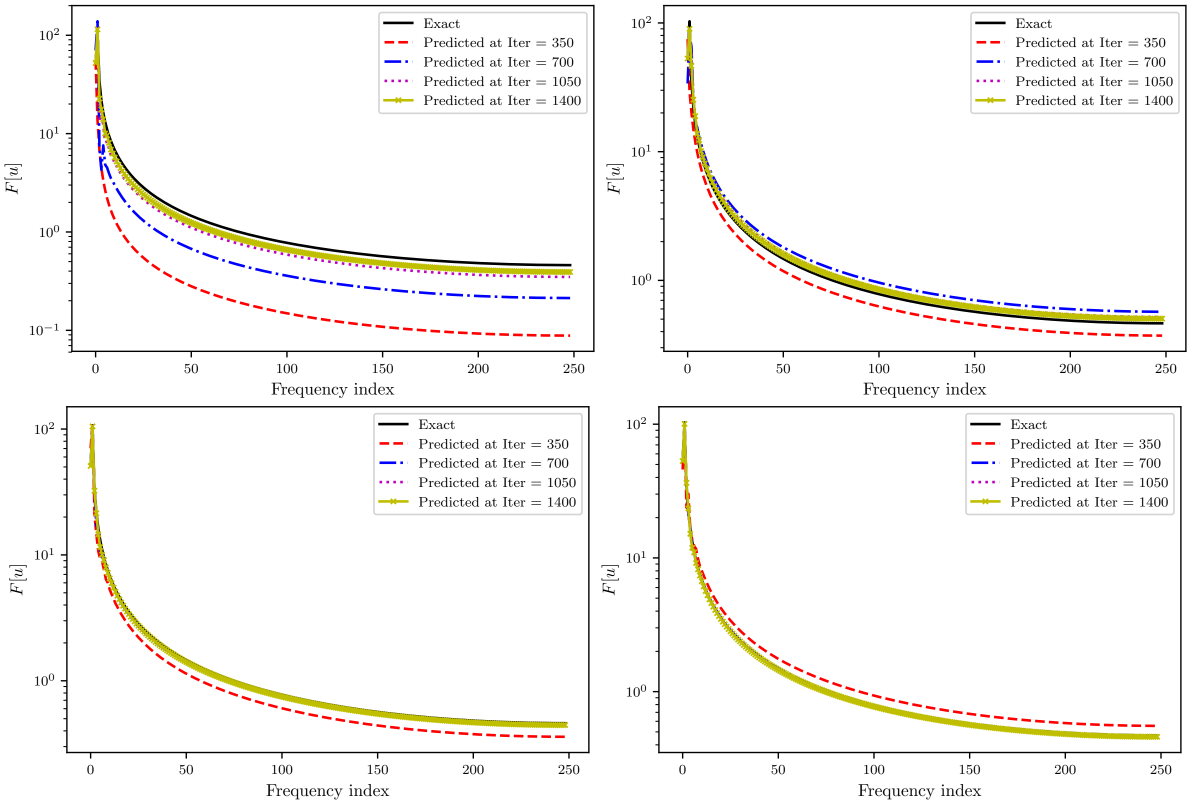

Figure 16: Comparison of solution of the Klein-Gordon equation in frequency domain with the fixed (1st row) and variable $a, n = 5$ (2nd row) *'tanh'* activation function. First column shows the frequencies in the solution at $x = -0.5$ whereas the second column shows the results at $x = 0.5$.

	$a = 1$	Variable a, $(n = 1)$	Variable a, $(n = 5)$	Variable a, $(n = 10)$
Relative L_2 error	1.953597e-01	1.026246e-01	9.528848e-02	9.064256e-02

Table 2: Klein-Gordon equation: Relative L_2 error after 1400 iterations with different values of a with clean data.

We plotted the solution at $x = -0.5$ and 0.5 (column-wise) in frequency domain and compared the results of fixed (top row) and adaptive activation (bottom row) functions as shown in figure 16. The adaptive activation function captures all frequencies contained in the solution much faster than the fixed activation function. In both cases, all frequencies are captured in 400 iterations (approximately) by the adaptive activation whereas the fixed activation takes more than 1500 iterations.

3.4. *Helmholtz equation*

The Helmholtz equation is one of the fundamental equations of mathematical physics arising in many physical problems like vibrating membranes, acoustics, electromagnetism equations, *etc*, see book by Sommerfeld [34] for more details. In two dimensions it is given by

$$\Delta u + k^2(u) = q(x, y), \quad (x, y) \in [-1,\ 1]^2 \tag{7}$$

with homogeneous Dirichlet boundary conditions. The forcing term is given by

$$q(x, y) = 2\pi\cos(\pi\, y)\sin(\pi\, x) + 2\pi\cos(\pi\, x)\sin(\pi\, y) + \ (x + y)\sin(\pi\, x)\sin(\pi\, y) - 2\pi^2(x + y)\sin(\pi\, x)\sin(\pi\, y)$$

The exact solution for $k = 1$ is

$$u(x, y) = (x + y)\sin(\pi\, x)\sin(\pi\, y).$$

In this case, the number of hidden layers is two and in each layer 40 neurons are used. The residual training points are 16000 whereas the N_u points are 400. Figure 17 shows the comparison of exact solution with that of PINN solution using fixed and adaptive ($n = 10$) activation functions at three different location given by the black dash line in the contour plot. The relative L_2 error calculated at the end of 3600th iteration is 1.0591e-1 using the fixed activation function and 7.1945e-2 in the case of adaptive activation. We can also see the solution in the frequency domain given by figure 18 using fixed (1st row) and variable $a, n = 10$ (2nd row) *'tanh'* activation function. We can observe that the adaptive activation function captures frequencies faster than the fixed one in both locations $x = -0.5$ (first column) and $x = 0.5$ (second column). Finally, figure 19 (left) shows the loss function comparison where we see the fast convergence of the adaptive activation as compared to the fixed activation, and figure 19 (right) shows the variation of a with number of iterations where the optimal value of a is close to 3.

3.5. Inverse problem for two-dimensional sine-Gordon equation

An inverse problem is formulated as estimating the function $u \in \mathcal{U}$ from the data $s \in \mathcal{S}$ where $s = T(u) + noise$. Here $\mathcal{U}, \mathcal{S}$ are topological vector spaces and $T : \mathcal{U} \to \mathcal{S}$ gives a mapping of a given function which gives rise to data in the absence of noise. Machine learning when applied to inverse problems can be framed as the problem of reconstructing a nonlinear mapping $T^* : \mathcal{S} \to \mathcal{U}$ such that it satisfies the pseudo-inverse property as $T^*(s) \approx u$ whenever data s is related to u. An important step in machine learning approaches is to parameterize the pseudo-inverse operator, and then the learning phase refers to choosing optimal parameters using some training data by minimizing a suitably defined loss function which gives the learned pseudo-inverse operator $T^*_{\tilde{\mathbf{\Theta}}}$. The training data are *iid* realizations of a $\mathcal{U} \times \mathcal{S}$-valued random variable (u, s) with known probability density function. This data is rich enough to allow a machine learning scheme to identify the structure of nonlinear mapping T given by the governing physical laws.

There are various approches proposed in the literature for a data-driven discovery of governing differential equations, for example, Raissi and Karniadakis [26] as well as Raissi et al. [30] in the context of Gaussian process, Rudy et al [33] proposed a sparse regression which is based on library of candidate terms and sparse model selection to select the important terms involved in the governing equation and recently by Berg and Nyström [7]. One of the efficient machine learning based approach for solving an inverse problem given by Raissi, et al. [28] is the data-driven discovery of partial differential equations by writing the governing equation as

$$u_{tt} + \mathcal{N}[u; \lambda] = 0 \tag{8}$$

where $\mathcal{N}[\cdot]$ contains parameterized linear/nonlinear terms. The network's job is to identify the unknown parameters $\lambda = \{\lambda_1, \lambda_2, \cdots\}$ as well as to obtain a qualitatively accurate reconstruction of the given solution. Here, we shall consider a two-dimensional sine-Gordon test case to solve the inverse problem where $N(u) = \phi\ \sin(u)$. In this test case $\phi = -1$ and the domain is $-7 \leq x, y \leq 7$. The initial conditions are given as

$$f(x, y) = 4\ \tan^{-1}(\exp(x + y))$$
$$g(x, y) = \frac{4(\exp(x + y))}{1 + (\exp(2x + 2y))}$$

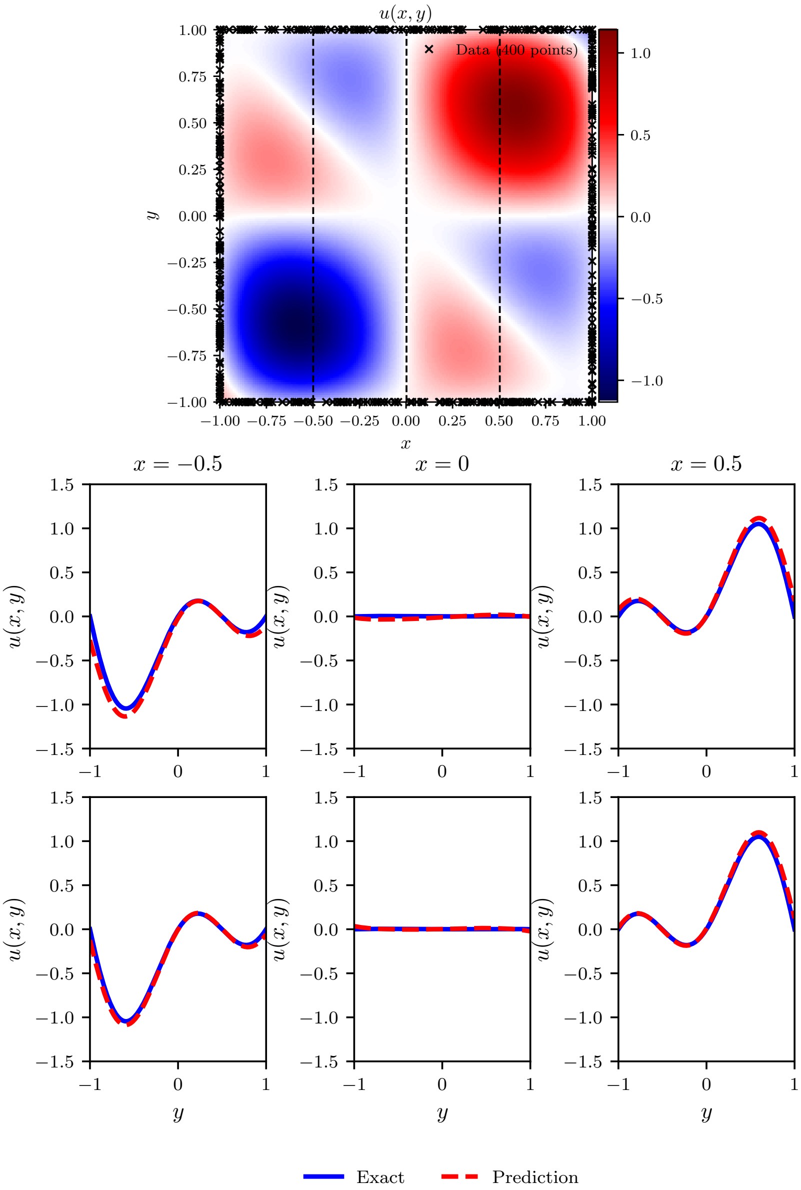

Figure 17: Contour plot (top) shows the solution of the Helmholtz equation using the adaptive activation function. The middle and bottom rows compare the PINN solution with exact solution using the fixed (middle) and variable $a, n = 10$ (bottom) 'tanh' activation function, respectively after 3600 iterations.

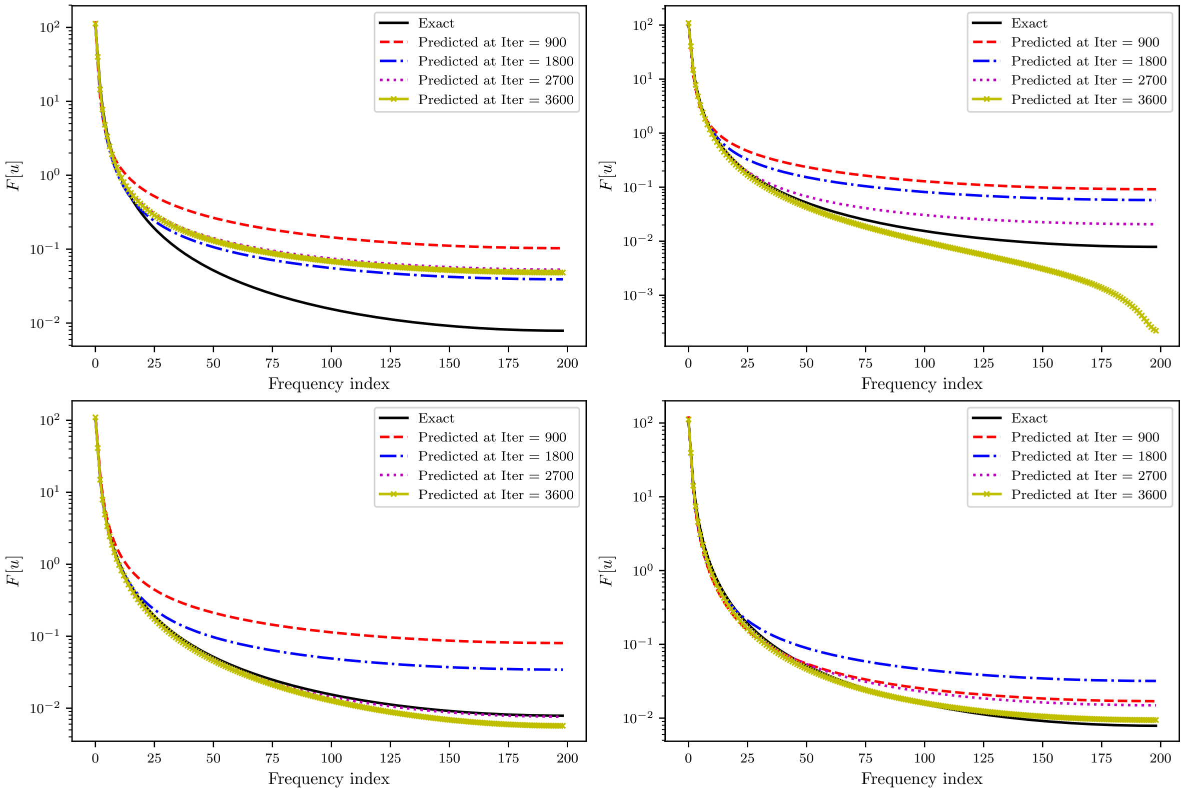

Figure 18: Comparison of solution of the Helmholtz equation in frequency domain using fixed (1st row) and variable $a, n = 10$ (2nd row) 'tanh' activation function. First column shows the frequencies in the solution at $x = -0.5$ location whereas second column shows the result at $x = 0.5$ location.

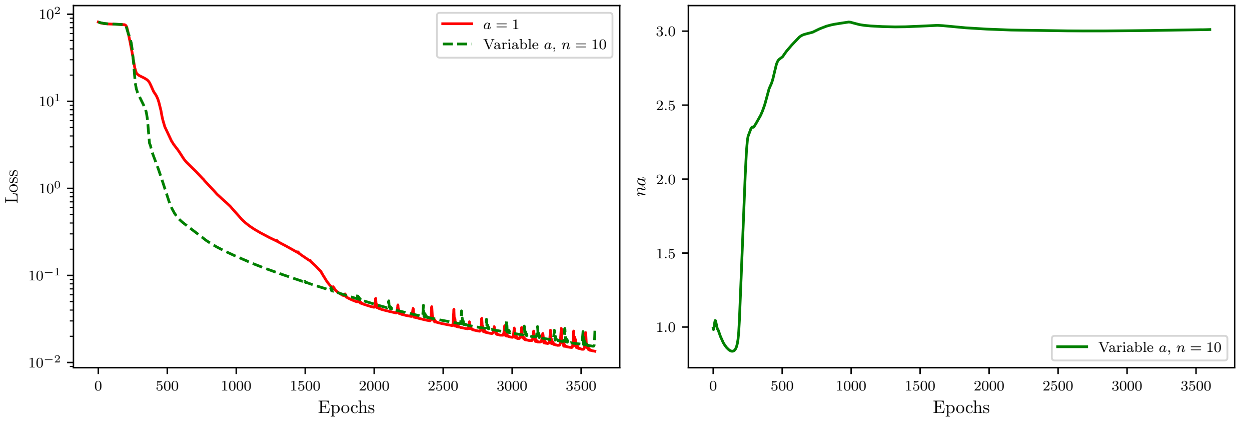

Figure 19: Helmholtz equation: (Left) loss function variation with epochs for fixed ($a = 1$) and (right) adaptive activation ($n = 10$) functions with variation in a.

and boundary conditions are

$$\frac{\partial u}{\partial x} = \frac{4(\exp(x+y+t))}{(\exp(2t)+\exp(2x+2y))} \quad \text{for } x = \pm 7 \text{ and } y \in [-7, 7],\ t \geq 0$$
$$\frac{\partial u}{\partial y} = \frac{4(\exp(x+y+t))}{(\exp(2t)+\exp(2x+2y))} \quad \text{for } y = \pm 7 \text{ and } x \in [-7, 7],\ t \geq 0$$

which has the analytical solution

$$u(x, y, t) = 4\ \tan^{-1}(\exp(x+y-t)).$$

In the case of the inverse problem, the loss function is the same as given by equation (2) but the MSE is given by

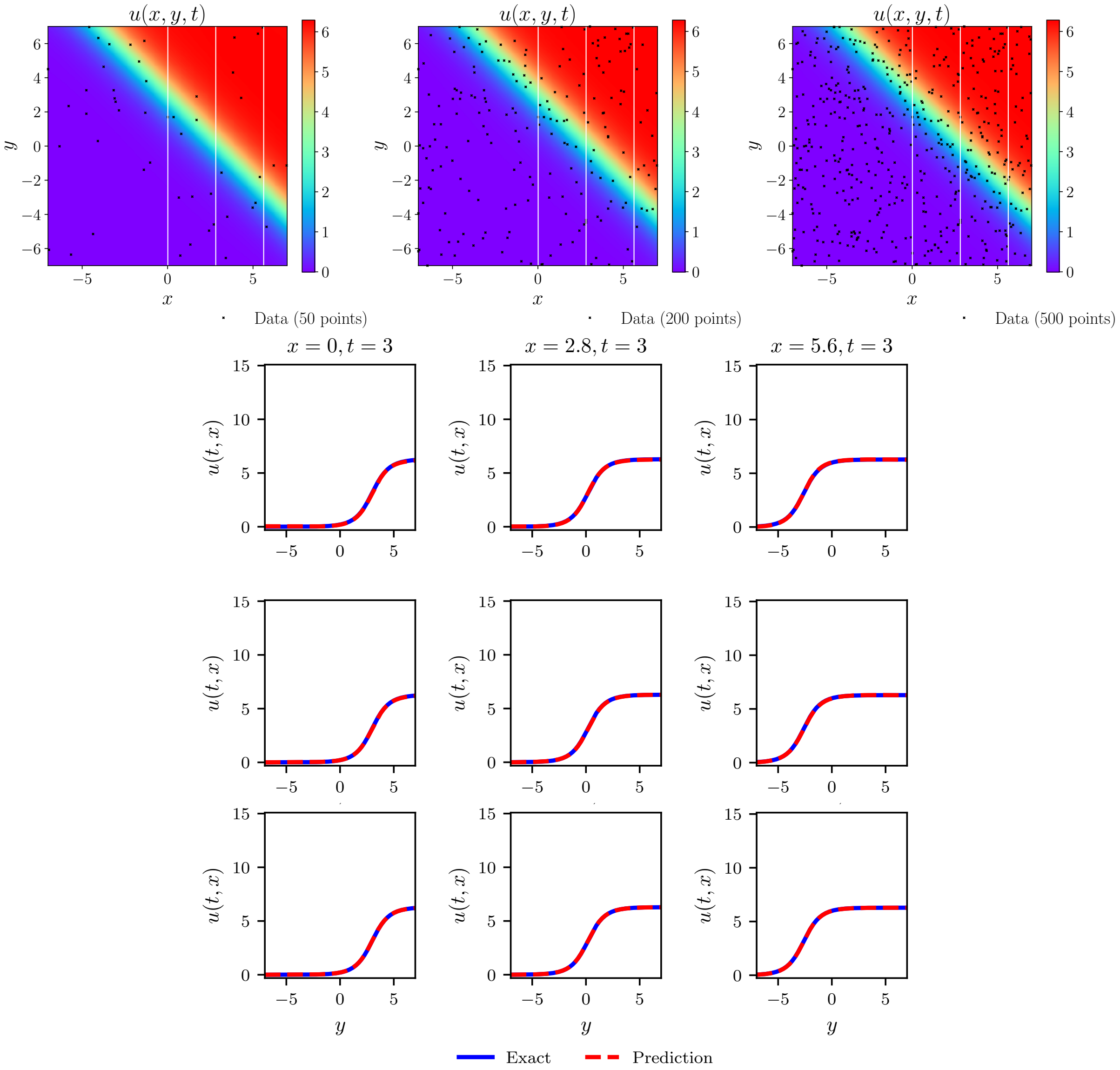

Figure 20: Contour plots of the PINN solution for two-dimensional sine-Gordon equation with adaptive activation function ($n = 5$) using $N_u = 50, 200$ and 500 (top row). The second, third and fourth rows compare the PINN solution with the exact one using $N_u = 50, 200$ and 500, respectively.

$$MSE_{\mathcal{F}} = \frac{1}{N_u}\sum_{i=1}^{N_u} |\mathcal{F}(x_u^i, y_u^i, t_u^i; \lambda_1, \lambda_2, \cdots)|^2, \quad MSE_u = \frac{1}{N_u}\sum_{i=1}^{N_u} |u^i - u(x_u^i, y_u^i, t_u^i)|^2.$$

Here $\{x_u^i, y_u^i, t_u^i\}_{i=1}^{N_u}$ denotes the training data points from the boundary as well as from inside the domain. The loss MSE_u corresponds to training data on the solution $u(x, y, t)$ whereas $MSE_{\mathcal{F}}$ enforces the governing equation on the same set of training data points. For our analysis, 50, 200 and 500 training data points, which are randomly selected points are used. The neural network architecture consists of four hidden layers with 20 neurons in each layer.

	$N_u = 50$			$N_u = 200$			$N_u = 500$		
	Clean	1% noise	2% noise	Clean	1% noise	2% noise	Clean	1% noise	2% noise
λ_1	3.28550	1.439983	3.218234	2.50646	0.831884	3.420329	1.04115	0.297201	1.896238
λ_2	1.15104	2.333641	2.443504	2.04701	2.199578	1.212937	1.24181	1.380813	0.351852
λ_3	0.50759	0.120240	0.495362	2.61289	1.729769	3.965372	0.64331	0.680488	1.020026
λ_4	1.08709	1.030558	1.178467	1.77241	1.530927	1.755536	0.92602	1.200277	1.376885

Table 3: Sine-Gordon equation: Percentage relative L_2 error in $\lambda_1 = 1, \lambda_2 = 1, \lambda_3 = 1$ and $\lambda_4 = 4$ for different N_u points using the adaptive activation function after 3500 iterations.

	$N_u = 500$ (fixed activation)			$N_u = 500$ (adaptive activation)		
	Clean	1% noise	2% noise	Clean	1% noise	2% noise
λ_1	6.25785	10.22437	7.876128	1.04115	0.297201	1.896238
λ_2	6.22453	7.21347	5.720103	1.24181	1.380813	0.351852
λ_3	8.99409	3.74553	9.965611	0.64331	0.680488	1.020026
λ_4	3.55075	4.54000	3.60425	0.92602	1.200277	1.376885

Table 4: Sine-Gordon equation: Comparison of percentage relative L_2 error in $\lambda_1 = 1, \lambda_2 = 1, \lambda_3 = 1$ and $\lambda_4 = 4$ obtained after 3500 iterations for the fixed and the adaptive activation functions using $N_u = 500$ points.

Correct PDE	$4\ s(x, y) - u_{xx} - u_{yy} + sin(u) = 0$
Identified PDE (Clean data)	$(3.85797)\ s(x, y) - (0.93743)\ u_{xx} - (0.93776)\ u_{yy} + (0.9100591)\ \sin(u) = 0$
Identified PDE (1 % noise)	$(3.81840)\ s(x, y) - (0.89776)\ u_{xx} - (0.92790)\ u_{yy} + (0.9625447)\ \sin(u) = 0$
Identified PDE (2 % noise)	$(3.85583)\ s(x, y) - (0.92124)\ u_{xx} - (0.94280)\ u_{yy} + (0.9003439)\ \sin(u) = 0$

Table 5: Sine-Gordon equation: Identification of two-dimensional sine-Gordon equation with the *fixed* activation function after 3500 iterations.

Correct PDE	$4\ s(x, y) - u_{xx} - u_{yy} + sin(u) = 0$
Identified PDE (Clean data)	$(3.96296)\ s(x, y) - (1.01041)\ u_{xx} - (0.98759)\ u_{yy} + (1.03064331)\ \sin(u) = 0$
Identified PDE (1 % noise)	$(3.95199)\ s(x, y) - (1.00297)\ u_{xx} - (0.98619)\ u_{yy} + (0.9931951)\ \sin(u) = 0$
Identified PDE (2 % noise)	$(3.94492)\ s(x, y) - (0.98104)\ u_{xx} - (0.99648)\ u_{yy} + (0.9897997)\ \sin(u) = 0$

Table 6: Sine-Gordon equation: Identification of two-dimensional sine-Gordon equation using the *adaptive* activation function with scaling parameter $n = 5$ after 3500 iterations.

For careful scrutinization of the performance of the proposed approach, we vary the noise level in the training data. Given the noisy measurements of the data (x^i, y^i, t^i, u^i), we are interested in learning the parameters $\lambda = \{\lambda_1, \lambda_2, \cdots\}$.

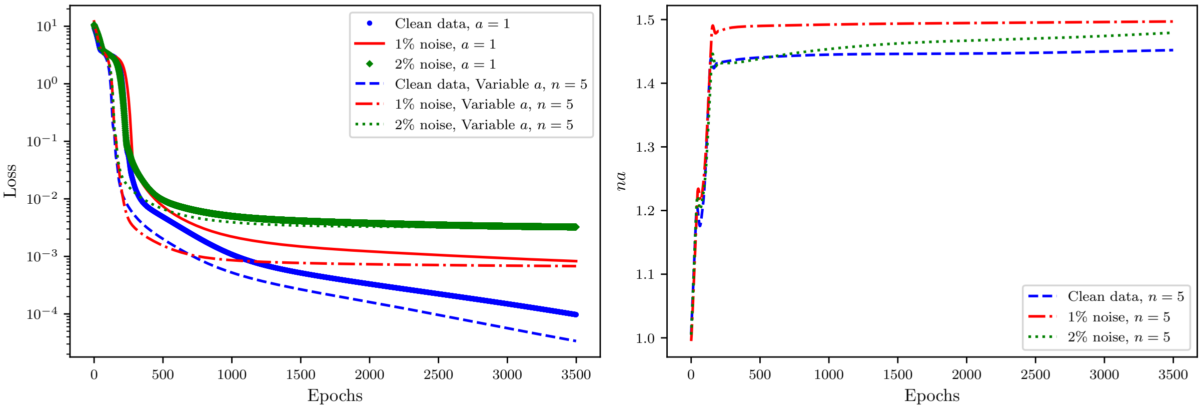

Figure 21: Sine-Gordon equation: Loss function (left) and variation of na (right) for clean data as well as data with noise using $N_u = 500$.

	Clean data	1 % error	2 % error
Fixed activation function	1.923454e-03	1.996804e-03	2.396984e-03
Adaptive activation function with $n = 5$	9.93412e-04	1.420345e-03	1.986455e-03

Table 7: Sine-Gordon equation: Comparison of relative L_2 error in the solution obtained after 3500 iterations for the fixed and the adaptable activation functions.

We define $\mathcal{F}$ as

$$\mathcal{F} := \lambda_4 \; s(x, y) - \lambda_1 u_{xx} - \lambda_2 u_{yy} + \lambda_3 \sin(u)$$

where the function $s(x, y)$ is given by

$$s(x, y) = \frac{e^{9+x+y} - e^{3+3(x+y)}}{\left(e^{6} + e^{2(x+y)}\right)^{2}}$$

and $\lambda_1 = \lambda_2 = \lambda_3 = 1, \lambda_4 = 4$.

Table 3 shows the percentage relative L_2 error in λ's for adaptive activation function using 50, 200 and 500 training data points. We observe that the error decreases with increase in training points. Moreover, in some λ's the error in the solution with 1% noise is slightly less than that of clean data. Figure 20 shows the solution of PINN using adaptive activation function for different N_u points, which accurately approximates the solution in the domain. Also, comparison of the PINN solution with the exact solution is considered at $x = 0, 2.8$ and 5.6 locations. Table 4 shows the comparison of percentage relative L_2 error in λ's using fixed and adaptive activation function after 3500 iterations. In the case of a fixed activation the maximum error is almost 9% in clean data whereas it is just 1.24% in adaptive activation function. This shows that the adaptive activation increases the accuracy of the solution. Table 5 shows the correct PDE along with the identified PDEs with clean data, 1% and 2% noise using the fixed activation function whereas table 6 shows the corresponding PDEs using the adaptive activation function, which is more accurate than its fixed counterpart. From the results we observe that the neural network is able to correctly identify the unknown parameters involved in the governing equations with very good accuracy even in the presence of noise in the training data. To quantify the accuracy we have given the relative L_2 error in table 7, which is again small for the adaptive activation function based PINN. Finally, the loss function using fixed and adaptive activation function is plotted for the three different data sets as shown in figure 21, which shows that the loss given by adaptive activation function based PINN converges faster.

4. Numerical results for standard deep learning benchmarks problems

In the previous sections, we have seen the advantage of adaptive activation functions with PINN for physics related problems. A natural question is then whether or not the advantage of adaptive activation remains with standard deep neural networks for other problems. To explore the question, this section presents experimental results with various standard deep learning benchmarks.

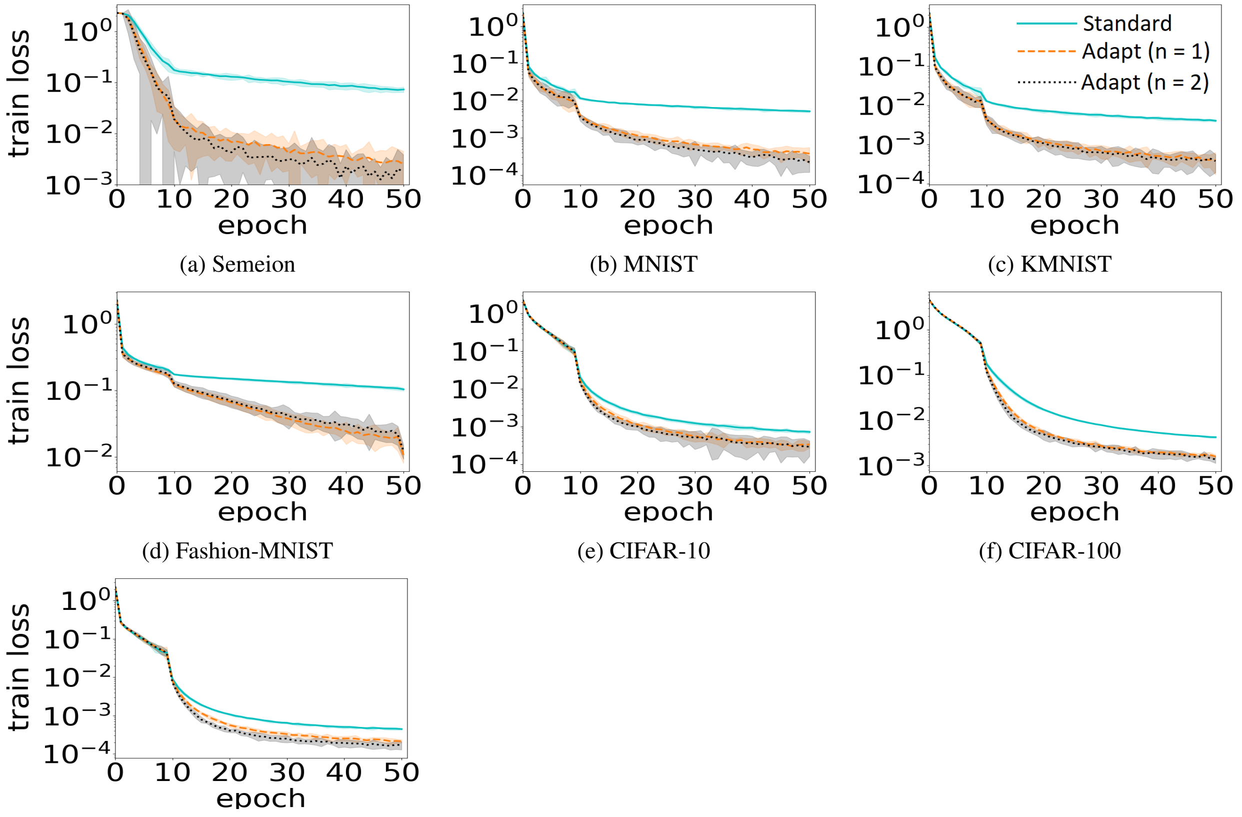

(a) Semeion

(b) MNIST

(c) KMNIST

(d) Fashion-MNIST

(e) CIFAR-10

(f) CIFAR-100

(g) SVHN

Figure 22: Training loss in log scale versus epoch for standard activation (solid blue line) and adaptive activation with $n = 1$ (dashed orange line) and $n = 2$ (dotted black line) without data augmentation.

Figures 22 and 23 show the mean values and the uncertainty intervals of the training losses for fixed activation function and adaptive activation function with the standard machine learning benchmarks. The solid and dashed lines are the mean values over ten random trials with random seeds. The shaded regions represent the intervals of 2×(the sample standard deviations) for each method. Figures 22 and 23 consistently show that adaptive activation accelerates the minimization of the training loss values with various machine learning datasets.

We used the standard cross entropy loss for training and plots. Pre-activation ResNet with 18 layers [16] was used for CIFAR-10, CIFAR-100, and SVHN datasets, whereas a standard variant of LeNet [18] with ReLU was used for other datasets; i.e., the architecture of the variant of LeNet consists of the following five layers (with the three hidden layers): (1) input layer, (2) convolutional layer with 64 5×5 filters, followed by max pooling of size of 2 by 2 and ReLU, (3) convolutional layer with 64 5×5 filters, followed by max pooling of size of 2 by 2 and ReLU, (4) fully connected layer with 1014 output units, followed by ReLU, and (5) Fully connected layer with the number of output units being equal to the number of target classes. All hyper-parameters were fixed a priori across all different datasets and models. We fixed the mini-batch size s to be 64, the initial learning rate to be 0.01, the momentum coefficient to be 0.9 and we use scaling factor $n = 1$ and 2. The learning rate was divided by 10 at the beginning of 10th epoch for all experiments (with and without data augmentation), and of 100th epoch for those with data augmentation.

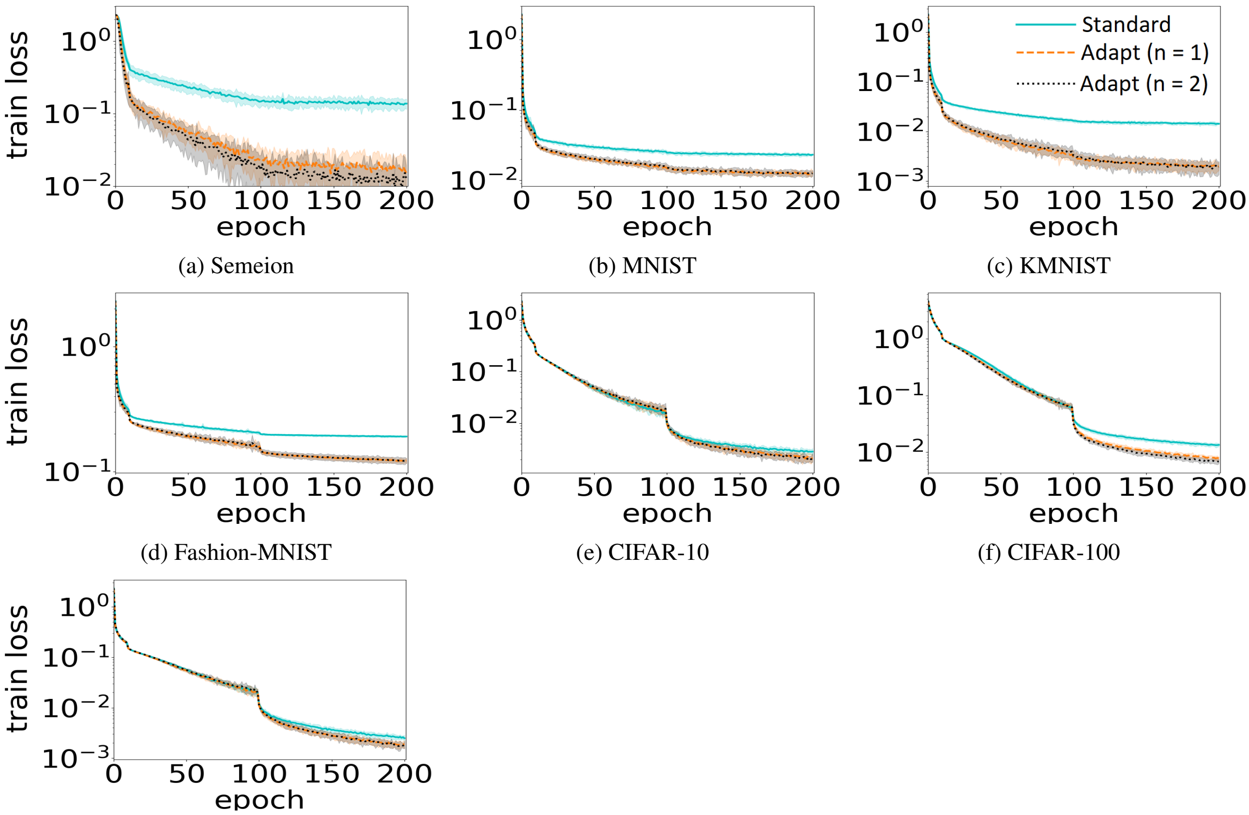

(a) Semeion

(b) MNIST

(c) KMNIST

(d) Fashion-MNIST

(e) CIFAR-10

(f) CIFAR-100

(g) SVHN

Figure 23: Training loss in log scale versus epoch for standard activation (solid blue line) and adaptive activation with $n = 1$ (dashed orange line) and $n = 2$ (dotted black line) with data augmentation.

5. Conclusions

Increasing the performance of deep learning algorithm is important in order to design fast and accurate machine learning techniques. By introducing the scalable hyper-parameter in the activation function, not only convergence of the neural network increases but also better accuracy is obtained. Thus, we can achieve a better performance of the neural network by the introduction of such parameter. To support our claim, various forward and inverse problems are solved using deep neural networks and physics-informed neural networks with smooth solution (given by Klein-Gordon equation, Helmholtz equation) as well as high gradient solution (given by the Burgers equation) in one and two dimensions. In all cases, it is shown that the decay in loss function is faster in the case of adaptive activation function, and correspondingly the relative L_2 error in solution is shown to be small in the proposed approach. In order to investigate the performance of such scalable hyper-parameter based adaptive activation function, the neural network solution is plotted in a frequency domain, revealing the capturing of the frequencies in the solution faster than fixed activation function. Moreover, the proposed adaptive activation function is shown to accelerate the minimization of the training loss values in standard deep learning benchmark problems with and without data augmentation. We theoretically proved that no suboptimal critical point or local minimum attract gradient descent algorithms in the proposed method under mild assumptions. The proposed approach can be used both in PINNs as well as in standard neural networks and is a promising and simple approach to increase the efficiency, robustness and accuracy of the neural network based approximation of nonlinear functions as well as the solution of partial differential equations, especially for forward problems.

Acknowledgement

This work was supported by the Department of Energy PhILMs grant DE-SC0019453, and by the DARPA-AIRA grant HR00111990025.

Appendix A. Proof of Theorem 2.1

We prove the statement by contradiction. Suppose that $\tilde{\mathbf{\Theta}} = \{w^k, b^k, a\}_{j=1}^D$ is a limit point of $(\tilde{\mathbf{\Theta}}_m)_{m\in\mathbb{N}}$ and a suboptimal critical point or local minimum.

Let $\ell_f^i := \varphi^i(u_{\tilde{\mathbf{\Theta}}}(\rho^i))$ and $\ell_u^i := |u^i - u_{\tilde{\mathbf{\Theta}}}(x_u^i, y_u^i, t_u^i)|^2$. Let $z_f^{i,k}$ and $z_u^{i,k}$ be the outputs of the k-th layer for ρ^i and (x_u^i, y_u^i, t_u^i), respectively. Define

$$h_f^{i,k,j} := na(w^{k,j} z_f^{i,k-1} + b^{k,j}) \in \mathbb{R},$$

and

$$h_u^{i,k,j} := na(w^{k,j} z_u^{i,k-1} + b^{k,j}) \in \mathbb{R},$$

for all $j \in \{1, \dots, N_k\}$, where $w^{k,j} \in \mathbb{R}^{1\times N_{k-1}}$ and $b^{k,j} \in \mathbb{R}$.

For all three cases of the conditions corresponding the different rules of the learning rate, from the proofs in [8, Propositions 1.2.1-1.2.4], we have that $\nabla J_\zeta(\tilde{\mathbf{\Theta}}) = 0$ and $J_\zeta(\tilde{\mathbf{\Theta}}) < J_\zeta(0)$. Thus, we have that for all $k \in \{1, \dots, D\}$ and all $j \in \{1, \dots, N_k\}$,

$$\begin{aligned}
&\partial_{w^{k,j}} J_\zeta(\tilde{\mathbf{\Theta}}) \\
&= \frac{na}{N_f} \sum_{i=1}^{N_f} (\partial_{h_f^{i,k,j}} \ell_f^i)(z_f^{i,k-1})^\top + \frac{na}{N_u} \sum_{i=1}^{N_u} (\partial_{h_u^{i,k,j}} \ell_u^i)(z_u^{i,k-1})^\top + 2\zeta w^{k,j}, \\
&= 0
\end{aligned}$$

and

$$\partial_{b^{k,j}} J_\zeta(\tilde{\mathbf{\Theta}}) = \frac{na}{N_f} \sum_{i=1}^{N_f} (\partial_{h_f^{i,k,j}} \ell_f^i) + \frac{na}{N_f} \sum_{i=1}^{N_f} (\partial_{h_u^{i,k,j}} \ell_u^i) + 2\zeta b^{k,j} = 0.$$

Furthermore,

$$\begin{aligned}
&\partial_a J_\zeta(\tilde{\mathbf{\Theta}}) \\
&= \frac{n}{N_f} \sum_{i=1}^{N_f} \sum_{k=1}^{D} \sum_{j=1}^{N_k} (\partial_{h_f^{i,k,j}} \ell_f^i)(w^{k,j} z_f^{i,k-1} + b^{k,j}) + \frac{n}{N_u} \sum_{i=1}^{N_u} \sum_{k=1}^{D} \sum_{j=1}^{N_k} (\partial_{h_u^{i,k,j}} \ell_u^i)(w^{k,j} z_u^{i,k-1} + b^{k,j}) \\
&= \sum_{k=1}^{D} \sum_{j=1}^{N_k} \frac{n}{N_f} \sum_{i=1}^{N_f} (\partial_{h_f^{i,k,j}} \ell_f^i)(w^{k,j} z_f^{i,k-1} + b^{k,j}) + \frac{n}{N_u} \sum_{i=1}^{N_u} (\partial_{h_u^{i,k,j}} \ell_u^i)(w^{k,j} z_u^{i,k-1} + b^{k,j}) \\
&= 0.
\end{aligned}$$

Therefore, since

$$\begin{aligned}
&w^{k,j}(\partial_{w^{k,j}} J_\zeta(\tilde{\mathbf{\Theta}}))^\top + b^{k,j}(\partial_{b^{k,j}} J_\zeta(\tilde{\mathbf{\Theta}})) - 2\zeta(\|w^{k,j}\|_2^2 + (b^{k,j})^2) \\
&= \frac{na}{N_f} \sum_{i=1}^{N_f} (\partial_{h_f^{i,k,j}} \ell_f^i) w^{k,j}(z_f^{i,k-1} + b^{k,j}) + \frac{na}{N_u} \sum_{i=1}^{N_u} (\partial_{h_u^{i,k,j}} \ell_u^i) w^{k,j}(z_u^{i,k-1} + b^{k,j}),
\end{aligned}$$

we have

$$\begin{aligned}
0 &= a(\partial_a J_\zeta(\tilde{\mathbf{\Theta}}))\\
&= \sum_{k=1}^{D}\sum_{j=1}^{N_k} w^{k,j}(\partial_{w^{k,j}} J_\zeta(\tilde{\mathbf{\Theta}}))^\top + b^{k,j}(\partial_{b^{k,j}} J_\zeta(\tilde{\mathbf{\Theta}})) - 2\zeta(\|w^{k,j}\|_2^2 + (b^{k,j})^2)\\
&= -2\zeta \sum_{k=1}^{D}\sum_{j=1}^{N_k} \|w^{k,j}\|_2^2 + (b^{k,j})^2,
\end{aligned}$$

which implies that $\sum_{k=1}^{D}\sum_{j=1}^{N_k}\|w^{k,j}\|_2^2 + (b^{k,j})^2 = 0$ since $\zeta \neq 0$. This implies that $w^{k,j} = 0$ and $b^{k,j} = 0$ for all k and j, and that $J_\zeta(\tilde{\mathbf{\Theta}}) = J_\zeta(0)$. This contradicts with $J_\zeta(\tilde{\mathbf{\Theta}}) < J_\zeta(0)$. □

References

[1] D. Arpit, et al., A closer look at memorization in deep networks, arXiv preprint arXiv:1706.05394, 2017.

[2] A.R. Barron, Universal approximation bounds for superpositions of a sigmoidal function. IEEE Trans. Inform. Theory, 39(3), 930-945, 1993.

[3] C. Basdevant, et al., Spectral and finite difference solution of the Burgers equation, Comput. Fluids, 14 (1986) 23-41.

[4] H. Bateman, Some recent researches on the motion of fluids, Monthly Weather Review, 43(4), 163-170, 1915.

[5] A.G. Baydin, B.A. Pearlmutter, A.A. Radul, J.M. Siskind, Automatic differentiation in machine learning: a survey, Journal of Machine Learning Research, 18 (2018) 1-43.

[6] Y. Bengio, Simard P. and Frasconi P., Learning long-term dependencies with gradient descent is difficult, IEEE Transactions on Neural Networks, 5(2), 157-166, 1994.

[7] J. Berg, K. Nyström , Data-driven discovery of PDEs in complex datasets, J. Comput. Phys. 384 (2019) 239-252.

[8] D.P. Bertsekas, Nonlinear programming, Athena scientific Belmont, 1999.

[9] J.M. Burgers,A mathematical model illustrating the theory of turbulence. In advances in applied mechanics, Vol. 1, pp. 171-199, 1948.

[10] P.J. Caudrey, I.C. Eilbeck, J.D. Gibbon, The sine-Gordon equation as a model classical field theory, Nuovo Cimento 25 (1975) 497-511.

[11] G. Cybenko, Approximations by superpositions of sigmoidal functions, Approximation theory and its applications, 9(3), 17-28, 1989.

[12] R.K. Dodd, I.C. Eilbeck, J.D. Gibbon, H.C. Morris, Solitons and Nonlinear Wave Equations, Academic, London, 1982.

[13] K. Duraisamy, Z.J. Zhang, A.P. Singh, New approaches in turbulence and transition modeling using data-driven techniques, AIAA paper 2015-1284, 2015.

[14] M. Dushkoff, R. Ptucha, Adaptive Activation Functions for Deep Networks, Electronic Imaging, Computational Imaging XIV, pp. 1-5(5).

[15] S.S. Haykin, Neural Networks: A comprehensive foundation, Prentice Hall, 1999.

[16] K. He, X. Zhang, S. Ren, J. Sun, Identity mappings in deep residual networks, European conference on computer vision, pp. 630-645, 2016.

[17] D. P. Kingma, J. L. Ba, ADAM: A method for stochastic optimization, arXiv:1412.6980v9, 2017.

[18] Y. LeCun, L. Bottou, Y. Bengio, P. Haffner, Gradient-based learning applied to document recognition, Proceedings of the IEEE, vol. 86, pp. 2278-2324, 1998.

[19] I.E. Lagaris, A. Likas, D.I. Fotiadis, Artifical neural network for solving ordinary and partial differential equations, IEEE Trans. Neural Networks, 9(5) 987-1000, 1998.

[20] B. Li, Y. Li and X. Rong, The extreme learning machine learning algorithm with tunable activation function, Neural Comput & Applie (2013) 22: 531-539.

[21] M. Minsky, S. Papert, Perceptrons, MIT Press, 1969.

[22] H. Owhadi, Bayesian numerical homogenization, Multiscale Model. Simul. 13, 812-828, 2015.

[23] E. J. Parish, K. Duraisamy, A paradigm for data-driven predictive modeling using field inversion and machine learning, J. Comput. Phys. 305, 758-774, 2016.

[24] S. Qian, et al, Adaptive activation functions in convolutional neural networks, Neurocomputing Volume 272, 10 January 2018, Pages 204-212.

[25] N. Rahaman, et al., On the spectral bias of deep neural networks, arXiv preprint arXiv:1806.08734, 2018.

[26] M. Raissi, G.E. Karniadakis, Hidden physics models: machine learning of nonlinear partial differential equations. J. Comput. Phys., 357, 125-141, 2018.

[27] M. Raissi, P. Perdikaris, G.E. Karniadakis, Numerical Gaussian processes for time-dependent and nonlinear partial differential equations. SIAM J. Sci. Comput. 40, A172-A198, 2018.

[28] M. Raissi, P. Perdikaris, G.E. Karniadakis, Physics-informed neural network: A deep learning framework for solving forward and inverse problems involving nonlinear partial differential equations. J. Comput. Phys., 378, 686-707, 2019.

[29] M. Raissi, P. Perdikaris, G.E. Karniadakis, Inferring solutions of differential equations using noisy multi-fidelity data, J. Comput. Phys. 335 (2017) 736-746.

[30] M. Raissi, P. Perdikaris, G.E. Karniadakis, Machine learning of linear differential equations using Gaussian processes, J. Comput. Phys., 348, 683-693, 2017.

[31] M. Raissi, Z. Wang, M.S. Triantafyllou, G.E. Karniadakis, Deep learning of vortex-induced vibrations, J. Fluid Mech. (2019), vol. 861, pp. 119-137.

[32] S. Ruder, An overview of gradient descent optimization algorithms, arXiv:1609.04747v2, 2017.

[33] S.H. Rudy, et al., Data-driven discovery of partial differential equations, Sci. Adv. 3(4), 2017.

[34] A. Sommerfeld, Partial Differential Equations in Physics, New York: Academic Press, 1949.

[35] Y. Shen, B. Wang, F. Chen and L. Cheng, A new multi-output neural model with tunable activation function and its applications, Neural Processing Letters, 20: 85-104, 2004.

[36] J.-X Wang, et al., A comprehensive physics-informed machine learning framework for predictive turbulence modeling, arXiv:1701.07102.

[37] A. Wazwaz, New traveling wave solutions to the Boussinesq and the Klein-Gordon equations, Communications in Nonlinear Science and Numerical Simulation 13 (2008), 889-901.

[38] G.B. Whitham, Linear and nonlinear waves, Vol. 42, John-Wiley & Sons, 2011.

[39] Z. Xu, Y. Zhang, T. Luo, Y. Xiao, Z. Ma, Frequency Principle: Fourier analysis sheds light on deep neural networks, arXiv:1901.06523v3, 2019.

[40] Yarotsky D., Error bounds for approximations with deep ReLU networks, Neural Networks, 94, 103-114, 2017.

[41] C. Yu, et al.,An adaptive activation function for multilayer feedforward neural networks, 2002 IEEE Region 10 Conference on Computers, Communications, Control and Power Engineering. TENCOM '02. Proceedings.

[42] Z.J. Zhang, K. Duraisamy, Machine learning methods for data-driven turbulence modeling, AIAA paper 2015- 2460, 2015.